Geomorphology 369 (2020) 107309

Contents lists available at ScienceDirect

Geomorphology

journal homepage: www.elsevier.com/locate/geomorph

Late Quaternary sedimentary processes in the central Arctic Ocean inferred from geophysical mapping

Lara F. Pérez [a,b,*], Martin Jakobsson [c], Thomas Funck [a], Katrine J. Andresen [d], Tove Nielsen [a], Matt O'Regan [c], Finn Mørk [a]

[a] Geological Survey of Denmark and Greenland (GEUS), Department of Geophysics, Øster Voldgade 10, 1350 Copenhagen K, Denmark
[b] British Antarctic Survey, High Cross, Madingley Road, Cambridge CB3 0ET, United Kingdom
[c] Stockholm University, Department of Geological Sciences, Svante Arrheniusväg 8 C, Geohuset Room R 209, 106 91 Stockholm, Sweden
[d] Aarhus University, Department of Geoscience, Høegh-Guldbergs Gade 2, 8000 Aarhus C, Denmark

ARTICLE INFO

Article history:
Received 27 February 2020
Received in revised form 12 May 2020
Accepted 15 June 2020
Available online 17 June 2020

Keywords:
Mass transport deposits
Sediment waves
Internal waves
Arctic Ocean

ABSTRACT

Cryospheric events in the Arctic Ocean have been largely studied through the imprints of ice sheets, ice shelves and icebergs in the seafloor morphology and sediment stratigraphy. Subglacial morphologies have been identified in the shallowest regions of the Arctic Ocean, up to 1200 m water depth, revealing the extent and dynamics of Arctic ice sheets during the last glacial periods. However, less attention has been given to sedimentary features imaged in the vicinity of the ice-grounded areas. Detailed interpretation of the sparse available swath bathymetry and sub-bottom profiles from the Lomonosov Ridge and the Amundsen Basin shows the occurrence of mass transport deposits (MTDs) and sediment waves in the central Arctic Ocean. The waxing and waning ice sheets and shelves in the Arctic Ocean have influenced the distribution of MTDs in the vicinity of grounding-ice areas, i.e. along the crest of Lomonosov Ridge. Due to the potential of Arctic sediments to hold gas hydrates, their destabilization should not be ruled out as trigger for sediment instability. Sediment waves formed by the interaction of internal waves that propagate along water mass interfaces with the bathymetric barrier of Lomonosov Ridge. This work describes the distribution and formation mechanisms of MTDs and sediment waves in the central Arctic Ocean in relation to grounding ice and internal waves between water masses, respectively. The distribution of these features provides new insight into past cryospheric and oceanographic conditions of the central Arctic Ocean.

1. Introduction

Many factors control patterns of sedimentation and influence the seafloor morphology and sediment stratigraphy of continental margins, submarine ridges and oceanic basins, from initial continental break-up and major movements of tectonic plates to sea-level oscillations (e.g. Potter and Szatmari, 2009; Lovell, 2010). In polar regions, seafloor morphology and stratigraphy are heavily influenced by the cryosphere. The variability of sea-ice, ice sheets, ice shelves and glaciers on seasonal, inter-annual and longer glacial-interglacial time scales have left imprints in the sedimentary record (e.g., Jakobsson et al., 2011; Bijl et al., 2018). Glacial induced morphologies on bathymetric highs in the Arctic Ocean were first mapped in the 1990s. First down to a water depth of 850 m on the Yermak Plateau north of Svalbard (Vogt et al., 1994) and subsequently close to the North Pole on the Lomonosov Ridge at water depths between 600 and 1000 m (Jakobsson, 1999). Glacial morphologies formed by scouring of deep-draft icebergs and ice shelves have since been extensively described in many studies (e.g. Polyak et al., 2001; Kristoffersen et al., 2004a; Dowdeswell et al., 2016; Jakobsson et al., 2014, 2016). The diversity of glacial morphologies on the Lomonosov Ridge indicates the grounding and flow of glacial ice across the ridge (e.g., Jakobsson et al., 2016; Stein et al., 2016). However, only a few studies describe the morphological seafloor and sub-bottom features located in the surroundings of the ice-grounded areas and adjacent deep abyssal plains (e.g. Kristoffersen et al., 2007; Mosher et al., 2010; Geissler et al., 2011; Polyak and Jakobsson, 2011; Castro et al., 2019). These features provide additional information on the processes occurring at the Arctic seafloor in relation to the grounding ice and the oceanographic pattern.

Here we focus on the late Quaternary processes that shaped the seafloor morphology and sub-bottom stratigraphy of the central Arctic Ocean, i.e. the Lomonosov Ridge and the Amundsen Basin. Mass transport deposits (MTDs) and sediment waves are discussed as sedimentary features, which reveal post-sedimentary instability or transport of

* Corresponding author at: British Antarctic Survey, High Cross, Madingley Road, Cambridge CB3 0ET, United Kingdom.
E-mail addresses: larrez@bas.ac.uk (L.F. Pérez), martin.jakobsson@geo.su.se (M. Jakobsson), tf@geus.dk (T. Funck), katrine.andresen@geo.au.dk (K.J. Andresen), tni@geus.dk (T. Nielsen), matt.oregan@geo.su.se (M. O'Regan), fm@geus.dk (F. Mørk).

https://doi.org/10.1016/j.geomorph.2020.107309

sediments in relation to recent tectonic, oceanographic or cryospheric influence in the central Arctic Ocean.

2. Background

Below, we introduce the regional context of the main sedimentary control factors of the Arctic Ocean.

2.1. Regional tectonic and sedimentary context

The Arctic Ocean consists of two main basins, the Amerasian and Eurasian basins. They are separated by the Lomonosov Ridge, which is an 1800 km long continental fragment that rifted from the Eurasian continental margin (e.g. Jokat et al., 1992; Brozena et al., 2003; Døssing et al., 2013). Following rifting, the Lomonosov Ridge experienced several phases of subsidence (Moran et al., 2006; O'Regan et al., 2008; Sangiorgi et al., 2008). At present, it is the most prominent bathymetric high of the Arctic Ocean (Fig. 1A), constituting a double-sided passive continental margin (e.g. Jokat et al., 1992; Cochran et al., 2006). The sedimentary record covering the Lomonosov Ridge is highly variable encompassing the past ~55 Myrs, but holding several hiatuses (Backman et al., 2006; Stevenson et al., 2015).

Seafloor spreading in the Eurasian Basin is still active at ultraslow spreading rates along the Gakkel Ridge (e.g. Brozena et al., 2003; Engen et al., 2003; Sohn et al., 2008; Pease et al., 2014; Nikishin et al., 2017). Enclosed between the Gakkel Ridge and the Lomonosov Ridge (Fig. 1), the Amundsen Basin hosts up to 4.5 km of sediments mainly derived from the Eurasian margin (Sekretov, 2002). Turbidity currents and hemipelagic sedimentation are the dominant depositional processes in the formation of the sedimentary record (Svindland and Vorren, 2002). At the base of the Lomonosov Ridge, the Amundsen Basin is partly occupied by a channel-fan system that has been referred to as the *North Pole Submarine Fan* (Kristoffersen et al., 2004b). Gravity driven flows have brought sediments from the Canadian and Greenland margins (Lincoln Sea) to the surroundings of the North Pole (Fig. 1A), following different trajectories since the fan formed in the Plio-Pleistocene (Kristoffersen et al., 2004b).

Mass transport deposits (MTDs) are additional products of gravity mass movements, and are frequent along continental margins (e.g. Mienert and Weaver, 2002; Shipp et al., 2011). MTDs form bodies of transparent or semi-transparent acoustic facies embedded in the stratified record (Reading, 1996). Their singular demarcation is highly dependent on the vertical resolution of the sub-bottom record. Many recognised MTDs in sub-bottom profiles could encompass several events, and therefore, they could be considered as mass transport complexes as defined by Pickering and Hiscot (2016). Globally, MTDs are associated with downslope transport due to the instability of sediments that can arise from several causes. Earthquakes and tectonic deformation are the most common triggers of slope instability resulting in the formation of MTDs (e.g. Masson et al., 2006). Destabilization of gas hydrates embedded in the sedimentary record can result in formation of MTDs (e.g. Mulder and Cochonat, 1996). On glaciated margins, MTDs may form in response to direct erosion by glacial ice, over-steepening of continental slopes due to high subglacial sediment supply, and isostatic rebound during rapid melting of ice sheets (e.g. Maslin et al., 2004; Masson et al., 2010; Mosher et al., 2010; Nelson et al., 2011). MTD triggers in the Arctic Ocean are generally unknown (e.g. Mosher et al., 2010), and likely vary substantially, but the seismicity due to isostatic rebound is potentially higher during deglacial phases (Mosher et al., 2012).

2.2. Regional oceanographic context

The oceanographic pattern of the Arctic Ocean changed from an estuarine circulation to an open-ocean setting during early Miocene, after the opening and deepening of the Fram Strait between Greenland and Svalbard (e.g. Jakobsson et al., 2007). Under the modern ventilated oceanographic circulation pattern, Atlantic Water enters from the northern North Atlantic Ocean and the Barents Sea, while Pacific Water flows in through the shallow Bering Strait (Fig. 1A) (Rudels, 2009). The Lomonosov Ridge separates the deep waters in the Amerasian and Eurasian basins and represents a threshold for intermediate water exchange (Anderson et al., 1994; Woodgate et al., 2001; Aksenov et al., 2011). However, there are several passages along the Lomonosov Ridge that allow throughflow of deep and intermediate waters (Björk et al., 2007, 2018; Rudels, 2009).

The water column of the Arctic Ocean is strongly stratified (e.g. Aksenov et al., 2011). The relatively warm (>0 °C) Atlantic Water occupies the water column between about 200 and 1000 m (e.g. Rudels et al., 2000). Below, the Arctic Intermediate Water spans the depth range from 1000 to 1500 m (Supplementary Fig. 1). The abyssal plains of the Eurasian Basin are occupied by the coldest Arctic Deep Water below 2000 m (Somavilla et al., 2013; Gemery et al., 2017). The oceanographic flow is characterized by a weak interior circulation and intensified boundary currents in the whole water column (Björk et al., 2018). Thus, the water masses flow from Siberia towards Greenland along the Lomonosov Ridge flank facing the Amundsen Basin (Fig. 1A) (Jones et al., 1995).

Current-related features such as contourite depositional systems can be formed under specific morphological and oceanographic conditions (e.g. Rebesco et al., 2014). One of the sedimentary products formed beneath water masses flowing along the seafloor are sediment waves (e.g. Wynn and Stow, 2002). Sediment waves are transverse, asymmetric bedforms of variable dimensions from tens of meters to a few kilometres wavelength and several meters high (Wynn et al., 2000). They are globally represented in continental margins (Wynn and Stow, 2002; Wynn and Masson, 2008). A combination of along-slope-flowing bottom currents and downslope-flowing turbidity currents are the most common processes invoked to explain the origin of sediment wave fields (Wynn and Stow, 2002). However, sediment waves can also form by internal waves between different water masses interacting with sloping seafloors and causing up-slope energy propagation and shear instability (Faugères et al., 2002; Pomar et al., 2012). The sedimentation patterns forming sediment waves are altered by increasing shear stresses due to the rise of near-bottom water velocities caused by internal waves (Cacchione et al., 2002).

2.3. Regional cryospheric context

The Arctic Ocean hosts the largest sea-ice extension in the Northern Hemisphere, which over time has been highly influenced by oceanographic conditions (e.g. Gladenkov et al., 2002; Marincovich and Gladenkov, 1999, 2001; Jakobsson et al., 2007; Stein et al., 2016), and climate (Polyak et al., 2010; Stein et al., 2012; Jakobsson et al., 2014). The late Miocene – early Pliocene change of tectonic boundary conditions may have made it possible for sea-ice over the central Arctic Ocean to reach near present-day summer extensions at 3.9 Ma (Knies et al., 2014). Furthermore, there is evidence that the Arctic sea-ice may have reached its modern winter extension at about 2.6 Ma (Raymo, 1994; Knies et al., 2014), coeval with the ramping up of large Northern Hemisphere glaciations. Since then, the sea-ice cover has evolved across the glacial-interglacial cycles of the Quaternary (e.g. Sarnthein et al., 2009), with 100 ka orbital cycles dominating for the last million years. At present, the seasonal oscillation of the sea-ice edge results in an ice coverage of ~15 million km^2 during winter and ~ 7 million km^2 remaining at the end of the summer melting (Fig. 1A) according to the records of the National Snow and Ice Data Center (NSIDC; https://nsidc.org/data/search/#keywords=sea+ice).

While traces of sea-ice are difficult to identify in the seafloor morphology, ridges and bathymetric highs in the central Arctic Ocean with crests shallower than ~1000 m have consistently been scoured by deep-draft glacier ice from icebergs calved from ice sheets and thick

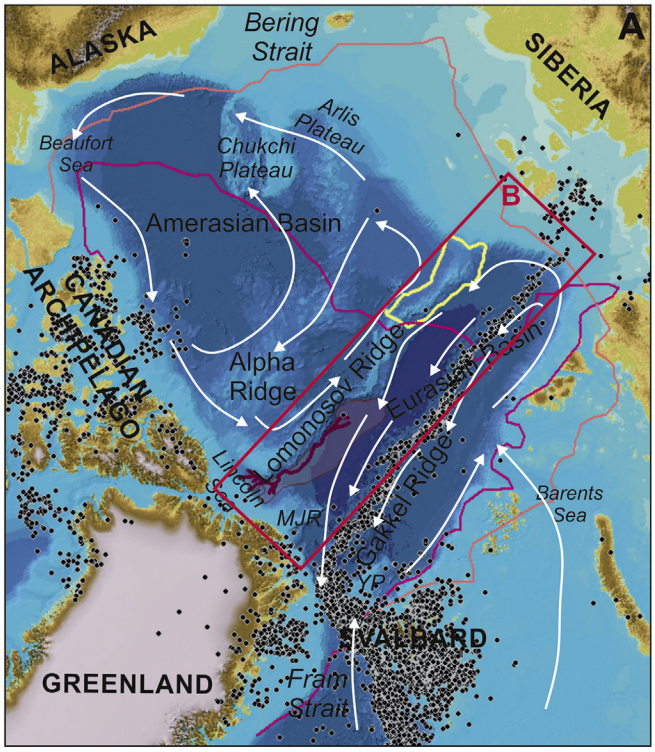
A
ALASKA
Bering Strait
SIBERIA
Arlis Plateau
Beaufort Sea
Chukchi Plateau
B
Amerasian Basin
CANADIAN ARCHIPELAGO
Alpha Ridge
Lomonosov Ridge
Eurasian Basin
Lincoln Sea
MJR
Gakkel Ridge
Barents Sea
YP
SVALBARD
GREENLAND
Fram Strait

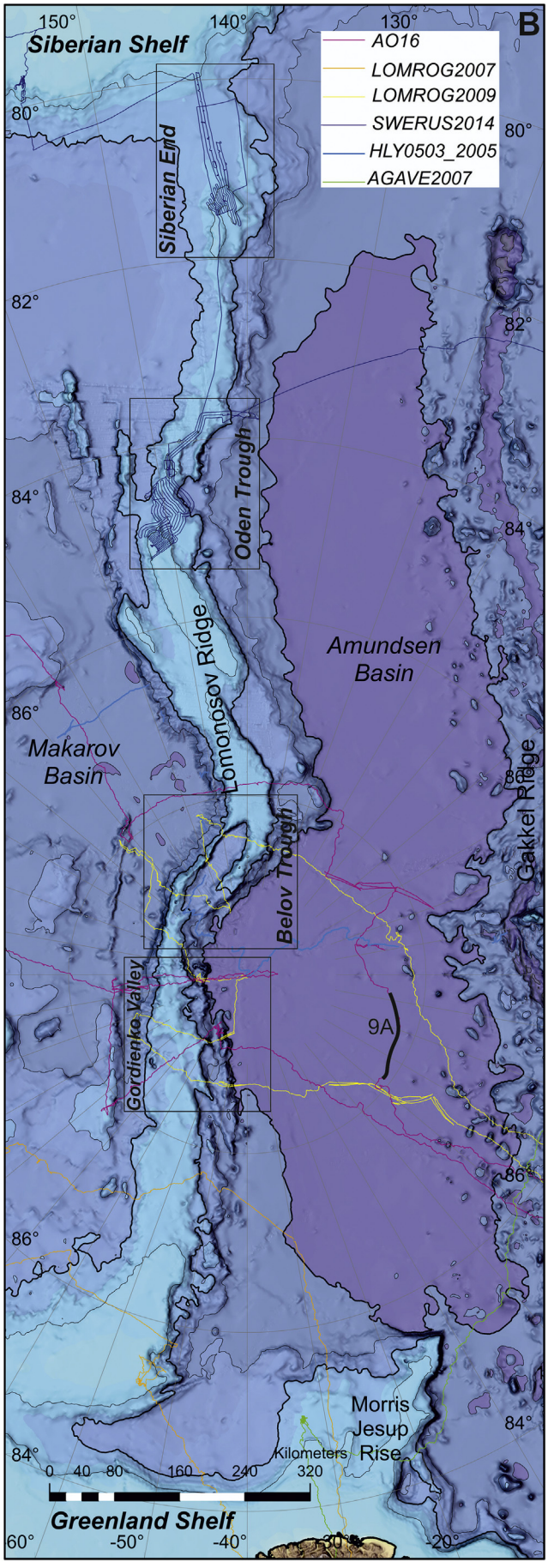
B
Siberian Shelf
AO16
LOMROG2007
LOMROG2009
SWERUS2014
HLY0503_2005
AGAVE2007
Siberian End
Oden Trough
Amundsen Basin
Lomonosov Ridge
Makarov Basin
Belov Trough
Gakkel Ridge
Gordienko Valley
9A
Morris Jesup Rise
Kilometers
0 40 80 160 240 320
Greenland Shelf
150°
140°
130°
80°
82°
84°
86°
60°
-50°
-40°
-30°
-20°

ice shelves (Jakobsson, 1999; Kristoffersen et al., 2007; Polyak et al., 2001; Jakobsson et al., 2014). The extension and thickness of ice sheets and ice shelves in the Arctic Ocean during past glacial periods has been a widely discussed topic over several decades (Mercer, 1970; Hughes et al., 1977; Grosswald and Hughes, 2008; Hebbeln et al., 1994; Sher, 1995; Polyak et al., 2001; De Vernal et al., 2005; Colleoni et al., 2009; Niessen et al., 2013; Jakobsson et al., 2014). Results from geophysical mapping and sediment coring show that the seafloor morphology of the Lomonosov Ridge, Chukchi Plateau, Arlis Plateau, Yermak Plateau and Morris Jesup Rise have been imprinted by grounding ice. The widespread evidence of glacial erosion in the Arctic Ocean has been interpreted in terms of the existence of a kilometre-thick ice shelf in the central Arctic Ocean at Marine Isotope Stage 6 (MIS 6) and possibly also during older glaciations (Jakobsson et al., 2016). However, ice biomarker proxies and climate simulations suggest open water areas along the Siberian margin during some intervals of MIS 6 (Stein et al., 2017). During the Last Glacial Maximum (LGM), corresponding to MIS 2, there are no clear signs of a thick and extensive ice shelf over the central Arctic Ocean (Jakobsson et al., 2014; Xiao et al., 2015; North Atlantic/Arctic Ocean Sea Ice Model) and open areas appear to have existed, judging from biologic productivity at several locations (Xiao et al., 2015; Gasson et al., 2018).

3. Methods

This work is based on the analysis of an extensive dataset of swath-bathymetry and sub-bottom profiles collected from the Lomonosov Ridge and adjoining Amundsen Basin (Fig. 1B, Fig. 2). The bulk of the data were acquired by Canada and the Kingdom of Denmark, as part of the mapping of the extended continental shelf within the framework of the United Nations Convention on the Law of the Sea (UNCLOS), in collaboration with the Swedish Polar Research Secretariat using the icebreaker (IB) *Oden* (Marcussen and the LOMROG II Scientific Party, 2009; Marcussen and the LOMROG III Scientific Party, 2012; Jakobsson et al., 2008). In addition, data from the SWERUS-C3 Expedition 2014 (Jakobsson et al., 2016) onboard IB *Oden*; and from the Healy–Oden Trans-Arctic Expedition (HOTRAX) 2005 with IB *Healy* and *Oden* (Darby et al., 2009) are included (Fig. 1B, Fig. 2). IB *Healy* has a Knudsen 320 3.5 kHz sub-bottom profiler that was used on the HOTRAX expedition. IB *Oden* is equipped with a Kongsberg SBP120 3° × 3° 2.5–7 kHz high-resolution chirp sub-bottom profiler. The penetration of the SBP120 into the sedimentary record is highly variable, but locally it exceeds 130 ms two-way travel-time (TWTT) below the seafloor, i.e. about 100 m of the sub-bottom sedimentary record are imaged. Interpretation of sub-bottom horizons has been performed in Petrel software (Schlumberger) and follows the basic interpretation criteria of seismo-stratigraphy (e.g. Payton, 1977). On the sub-bottom data, MTDs and sediment waves are identified on individual sub-bottom profiles. Sediment wave fields are mapped by visual correlation of these features on adjoining sub-bottom profiles. Depth and thickness maps in TWTT of key sub-bottom surfaces and layers have been produced in Petrel software using standard kriging interpolation on a 50 × 50 m grid. The multibeam echosounder is a Kongsberg EM122 1° × 1° 12 kHz. The transmitting transducer arrays for both the multibeam and sub-bottom profiler are protected from ice using polyurethane titanium reinforced windows. This limits the maximum multibeam swath width to ~60° coverage. On the multibeam grids, the swaths overlapped between 50 and 100%. The swath bathymetry has been gridded to a cell size of 20 m in ArcGIS software. Expendable bathythermograph (XBTs; Sippican) casts and conductivity-temperature-depth (CTD; SeaBird911 sensor suite) profiles were used for sound speed correction of the multibeam data. The multibeam data were processed using CARIS and Fledermaus-QPS software as described in Jakobsson et al. (2016) and Björk et al. (2018). Time-depth conversions of the sub-bottom profiles have been done using an average sound speed of 1600 m/s in the sediments as calculated by O'Regan et al. (2017) from the SWERUS cores located on the East Siberian continental margin. Ocean Data View (ODV) software has been used to visualize the hydrographic and oceanographic properties of the targeted areas (Supplementary Fig. 1).

4. Results

Due to the broad extension of the study area, the description of the identified sedimentary features is divided into four areas along the Lomonosov Ridge in addition to the Amundsen Basin (Fig. 1B, Fig. 2). The four areas at the Lomonosov Ridge are named after prominent nearby morphological features identified on the International Bathymetric Chart of the Arctic Ocean (IBCAO) Version 3.0 (Jakobsson et al., 2012). Moving from Greenland to Siberia, these four regions are: Gordienko Valley, Belov Trough, Oden Trough and Siberian End (referring to the Siberian End of Lomonosov Ridge).

In the Gordienko Valley and the Belov Trough, the imaged sedimentary record is relatively homogeneous, whereas three acoustic units can be distinguished on the sedimentary record of the Oden Trough and the Siberian End (Fig. 3, Fig. 4). The upper acoustic unit is relatively thin and formed of stratified sediments. It is referred to as the '*stratified-layer*' and has an average thickness of 4 m in the Oden Trough area and 12 m at the Siberian End (Fig. 3B, Fig. 4B). It is located over an acoustically transparent unit referred to as the '*blank-layer*' (Fig. 3, Fig. 4). The blank-layer has a maximum thickness of 48 m and an average thickness of 8 m in the surroundings of Oden Trough, and an average thickness of 24 m at the Siberian End reaching a maximum of 120 m (Fig. 3C, Fig. 4C). A third acoustic unit characterized by lateral continuous reflections can be identified in the sedimentary record above the attenuation of the acoustic signal. The reflections of this unit are commonly tilted and truncated at the top (Fig. 3A, Fig. 4A). The average burial depth of this truncation surface is roughly 12 m and 40 m in the Oden Trough and at the Siberian End, respectively (Fig. 3D, Fig. 4D). The sedimentary record of the Lomonosov Ridge and the Amundsen Basin is locally disturbed by numerous sedimentary features (Fig. 2, Fig. 5), including MTDs and sediment waves.

4.1. Mass transport deposits

MTDs are represented by local bodies of transparent to semi-transparent acoustic facies. They present lenticular shapes of a wide range of sizes and are found either embedded in the stratified pattern or outcropping at the seafloor (Fig. 2, Fig. 5B, Fig. 6, Fig. 7). In this study, a total of 123 MTDs are identified within the upper sedimentary record of the Lomonosov Ridge. Only a few of them (8) are located on the deep flank facing the Amundsen Basin, at average water depths of 2800 m (Fig. 8B). In the surroundings of the Gordienko Valley, the

Fig. 1. A) Overview of the Arctic Ocean based on the International Bathymetric Chart of the Arctic Ocean (IBCAO Version 3.0; Jakobsson et al., 2012). Dots show the location of earthquakes (catalogue of the International Seismological Centre, ISC). The light pink line indicates the average summer sea-ice boundary for the time period from 1981 to 2010 while the dark pink line represents the minimum sea-ice boundary in 2007 according to the National Snow and Ice Data Center (NSIDC). The yellow line represents the extension of the Bottom Simulator Reflector (BSR) identified in several multichannel seismic reflection profiles by Jokat (2005). The shaded area with the brown outline marks the *North Pole Submarine Fan* as interpreted by Kristoffersen et al. (2004a, 2004b). White arrows show the general intermediate oceanographic circulation from Rudels (2009). The red square indicates the study area shown in Fig. 1B. YP, Yermak Plateau; MJR, Morris Jesup Rise. B) Database of this study shown together with the bathymetry of the Lomonosov Ridge and Amundsen Basin based on the International Bathymetric Chart of the Arctic Ocean (IBCAO; Jakobsson et al., 2012), the contour interval is 1000 m (2000 and 4000 m in bold). The frames mark the location of the four main areas discussed in the manuscript (Gordienko Valley, Belov Trough, Oden Trough and Siberian End). Black line indicates the location of the sub-bottom profiles shown in Fig. 9A. (For interpretation of the references to colour in this figure legend, the reader is referred to the web version of this article.)

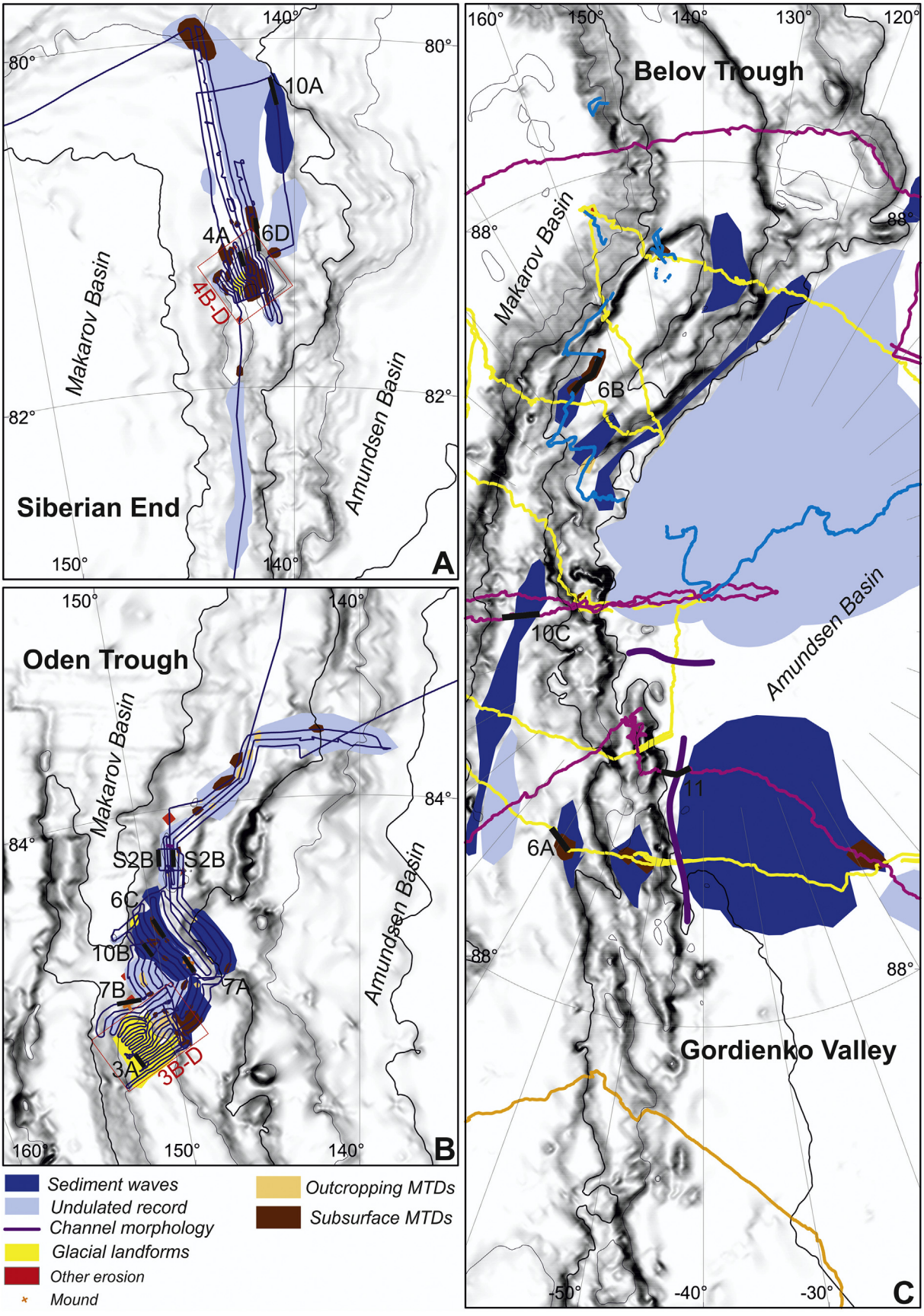

Fig. 2. Study areas over Lomonosov Ridge on the International Bathymetric Chart of the Arctic Ocean (IBCAO; Jakobsson et al., 2012) with a contour interval of 1000 m (2000 and 4000 m in bold). The main sedimentary features and mass transport deposits (MTDs) discussed in this work are represented. The colour lines represent the track lines of the ship navigation of the considered expeditions, legend as in Fig. 1B. A) Siberian End; B) Oden Trough; C) Belov Trough and Gordienko Valley. Black lines indicate the location of the sub-bottom profiles shown in following figures.

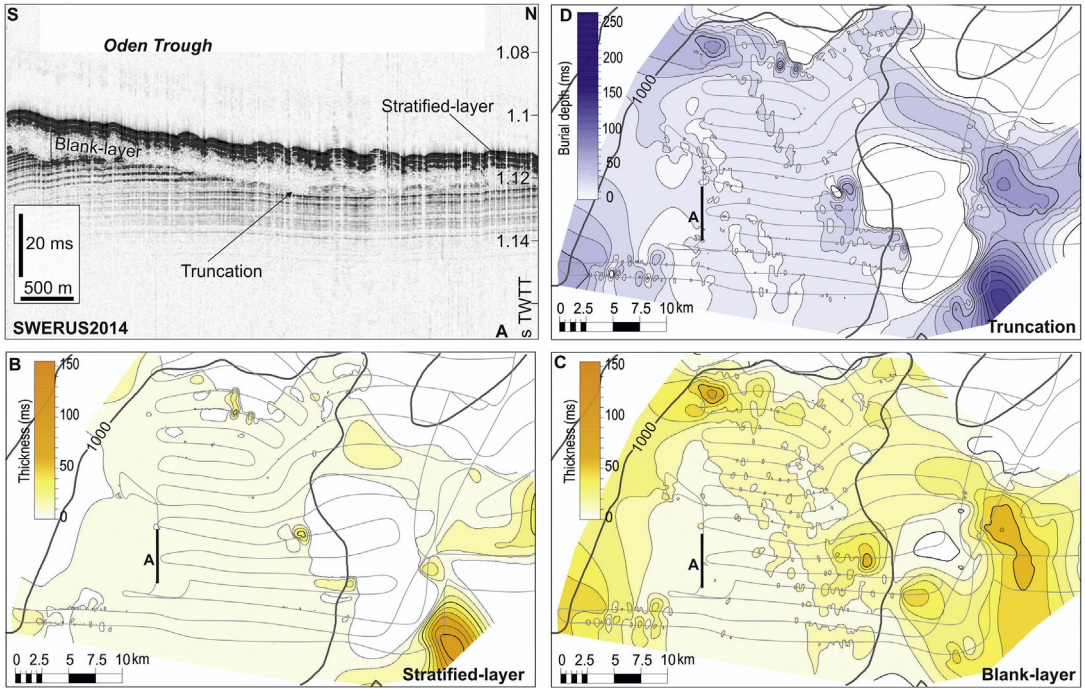

Fig. 3. A) Sub-bottom profile from the SWERUS2014 expedition in Oden Trough showing the stratified-layer, the blank-layer and the truncation surface discussed in the text. For location see Fig. 2B. TWTT, two-way travel-time. B) Thickness map of the stratified-layer. C) Thickness map of the blank-layer. D) Burial depth of the truncations. Thickness and depth are in TWTT. The thin grey lines represent the track lines of the ship navigation.

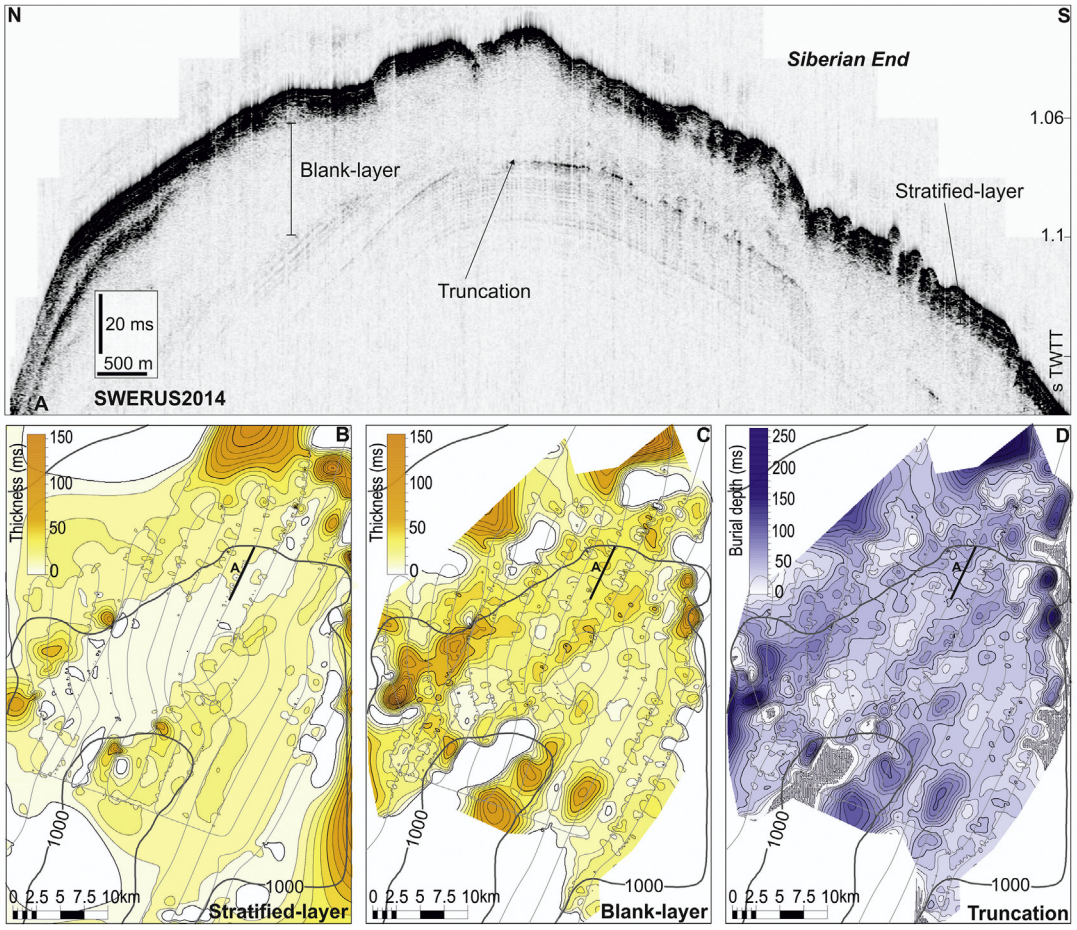

Fig. 4. A) Sub-bottom profile from the SWERUS2014 expedition at the Siberian End showing the stratified-layer, the blank-layer and the truncation surface discussed in the text. For location see Fig. 2B. TWTT, two-way travel-time. B) Thickness map of the stratified-layer. C) Thickness map of the blank-layer. D) Burial depth of the truncations. Thickness and depth are in TWTT. The thin grey lines represent the track lines of the ship navigation.

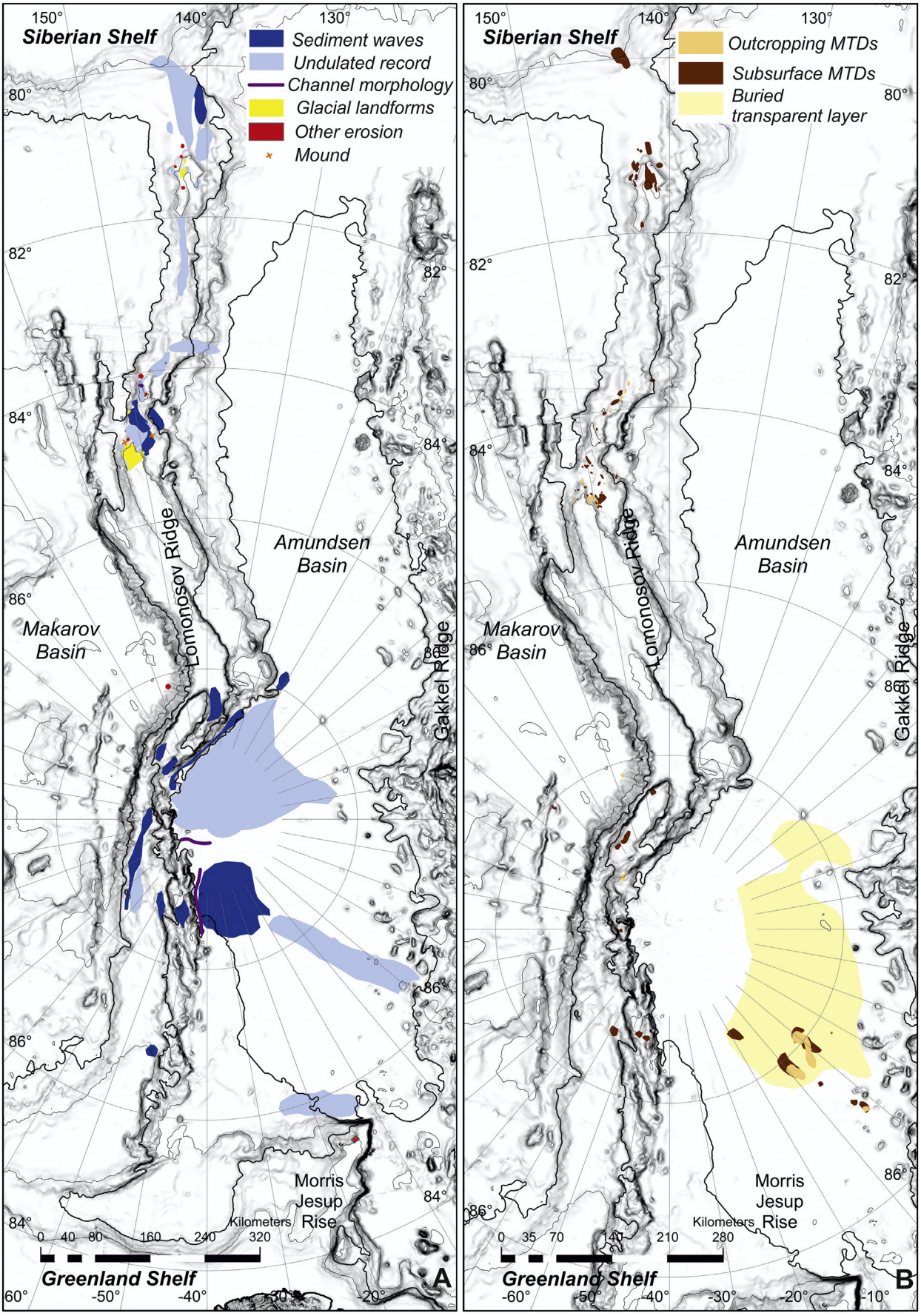

Fig. 5. International Bathymetric Chart of the Arctic Ocean (IBCAO; Jakobsson et al., 2012) with a contour interval of 1000 m (2000 and 4000 m in bold). A) Main sedimentary features discussed in this work. B) Mass transport deposits (MTDs).

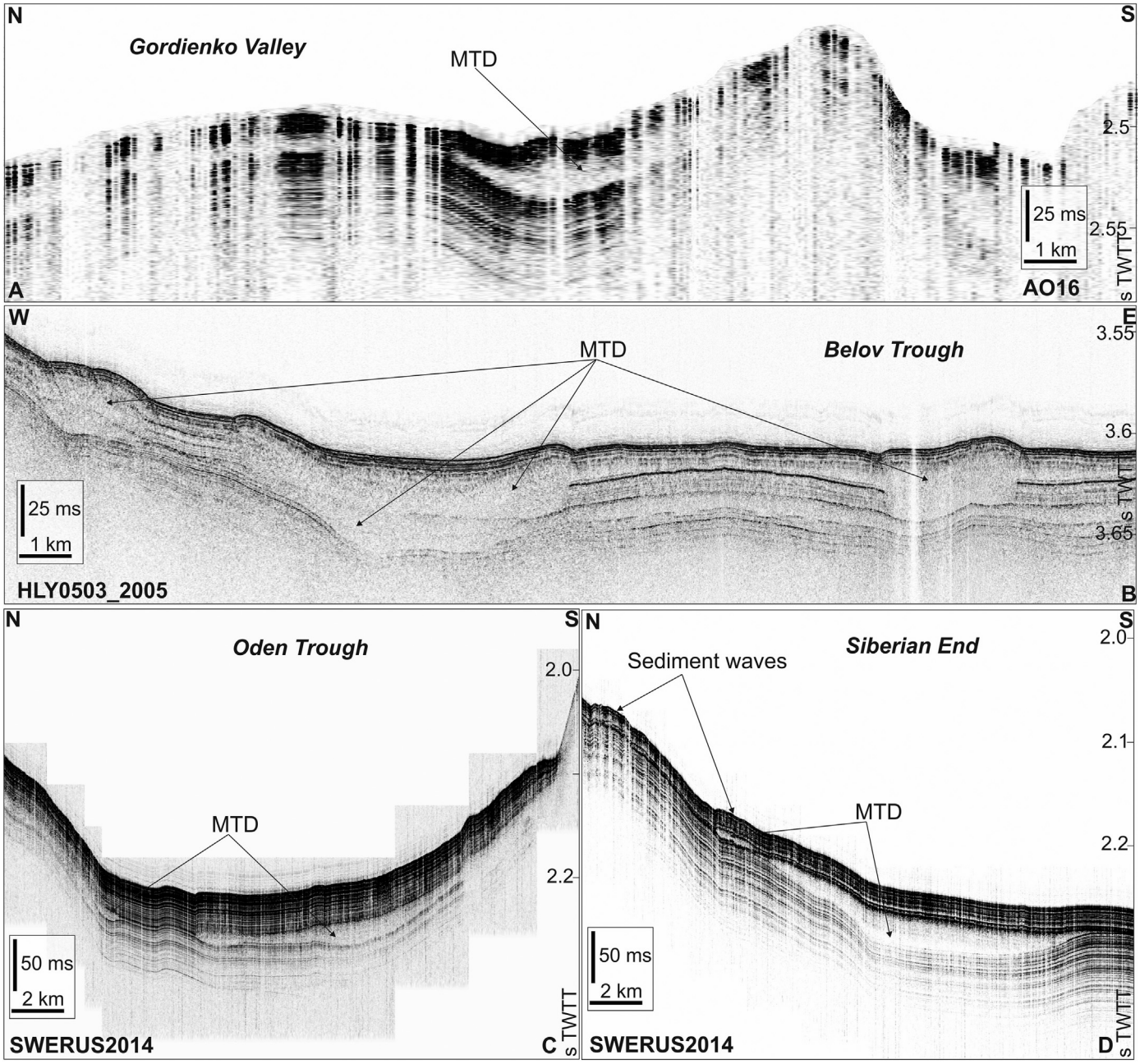

Fig. 6. Examples of identified mass transport deposits (MTDs). For location see Fig. 2B. TWTT, two-way travel-time. A) Gordienko Valley, sub-bottom profile from the AO16 expedition; B) Belov Trough, sub-bottom profile from the HOTRAX expedition; C) Oden Trough, sub-bottom profile from the SWERUS2014 expedition; D) Siberian End, sub-bottom profile from the SWERUS2014 expedition.

identified MTDs have maximum lengths of 4.3 km and 12 m maximum thickness (Fig. 6A, Fig. 8A). Adjacent to the Belov Trough, the MTDs have maximum lengths of 7.7 km and 23 m maximum thickness (Fig. 6B, Fig. 8A). The burial depths of the MTDs are on average 11 m in the Gordienko Valley, and 3.8 m in the Belov Trough, where a single outcropping MTD is also identified (Fig. 8C).

MTDs are more abundant along the crest of the Lomonosov Ridge (115), where they are prolific in the vicinity of the Oden Trough (54) and on the Siberian End (61). The MTDs located in the Oden Trough area are found at an average water depth of 1463 m (Fig. 8B). They have a maximum length of 11 km and a maximum thickness of 44 m, but in average, they are 2.7 km long and 12 m thick (Fig. 6C, Fig. 8A). The burial depths of the MTDs in the Oden Trough are 8.3 m in average (Fig. 8C). However, outcropping MTDs are particularly abundant in this area (18 out of 54). Some of the MTDs identified in Oden Trough are adjacent to mound-like formations placed at water depths of ~1500 m (Fig. 5A, Fig. 7). On the Siberian End, the MTDs are located in areas of average water depth of 1127 m, where the largest MTDs are 3.7 km long and 80 m thick, but the average is a length of 2 km and a thickness of 13 m (Fig. 6D, Fig. 8A, B). None of the identified MTDs in the Siberian End are outcropping at the seafloor; their average burial depth is 14 m (Fig. 8C).

In the upper sedimentary record of the Amundsen Basin, a total of 13 MTDs are identified. They have a lenticular shape and are concentrated near Gakkel Ridge (Fig. 5B, Fig. 9A). The largest body is over 47 km long and 12 m thick, but in average they are 11.7 km long and 4.6 m thick (Fig. 8A). Four of the MTDs are outcropping at the seafloor, but in general, they are placed within the upper most 10 m of the sedimentary record, buried at 2.9 m in average (Fig. 8C, Fig. 9A). An acoustic unit of transparent facies occupies the flat abyssal plain of the Amundsen

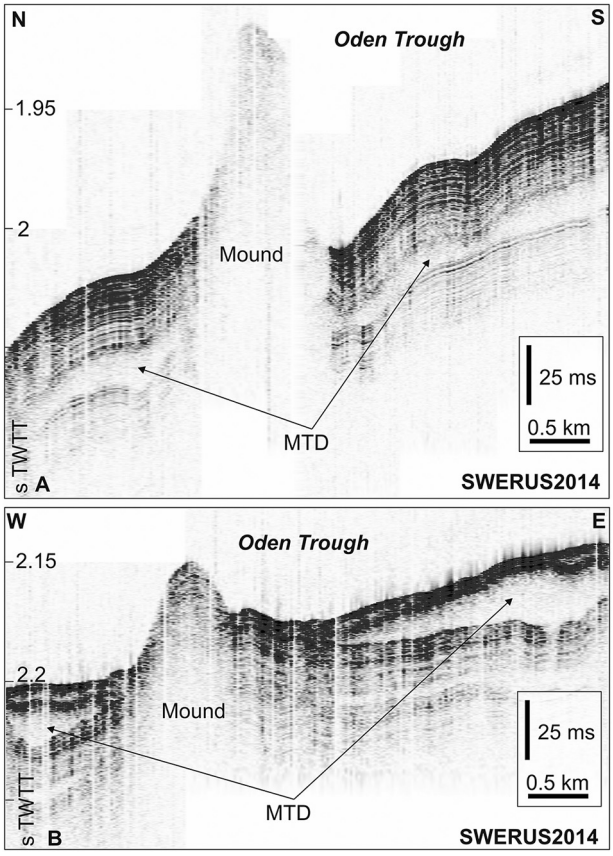

Fig. 7. Sub-bottom profile examples of mass transport deposits (MTDs) in the vicinity of mound morphologies in Oden Trough. Data from expedition SWERUS2014. For location see Fig. 2B. TWTT, two-way travel-time.

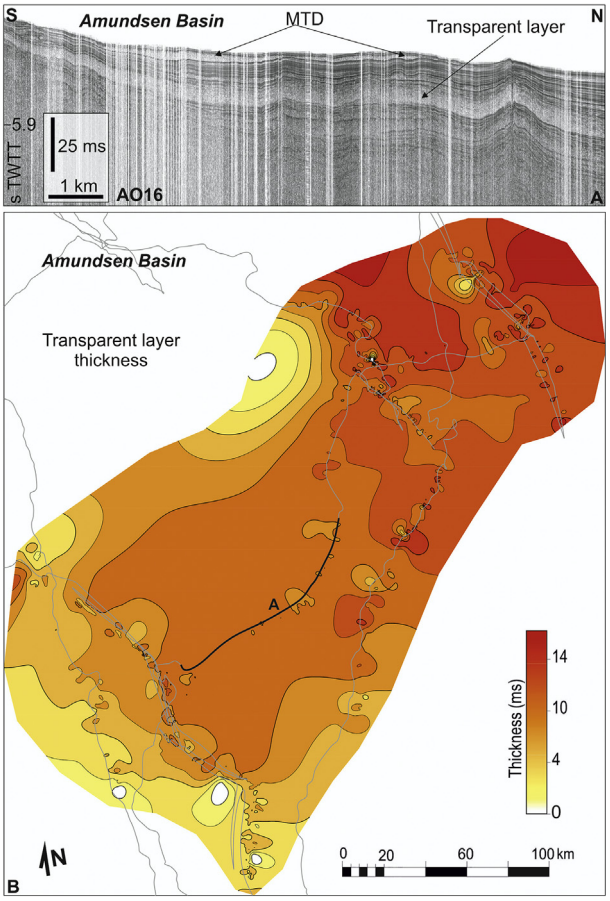

Fig. 9. A) Sub-bottom profile from the expedition AO16 across Amundsen Basin showing mass transport deposits (MTDs) and the transparent layer. For location see Fig. 1B and Fig. 9B. B) Thickness distribution of the transparent layer in Amundsen Basin in ms two-way travel-time (TWTT). The thin grey lines represent the track lines of the ship navigation.

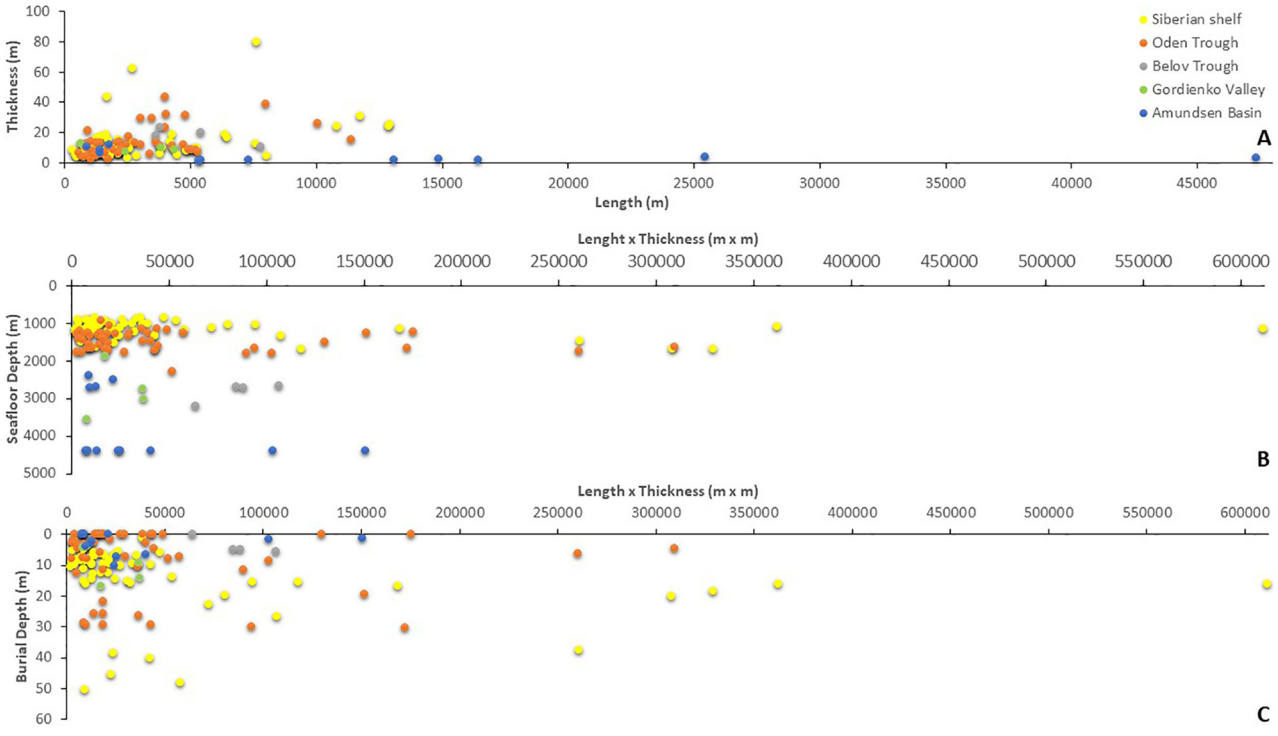

Fig. 8. Properties of the identified mass transport deposits (MTDs) by location area. A) Thickness vs. length; B) water depth vs. size (length × thickness); c) burial depth vs. size.

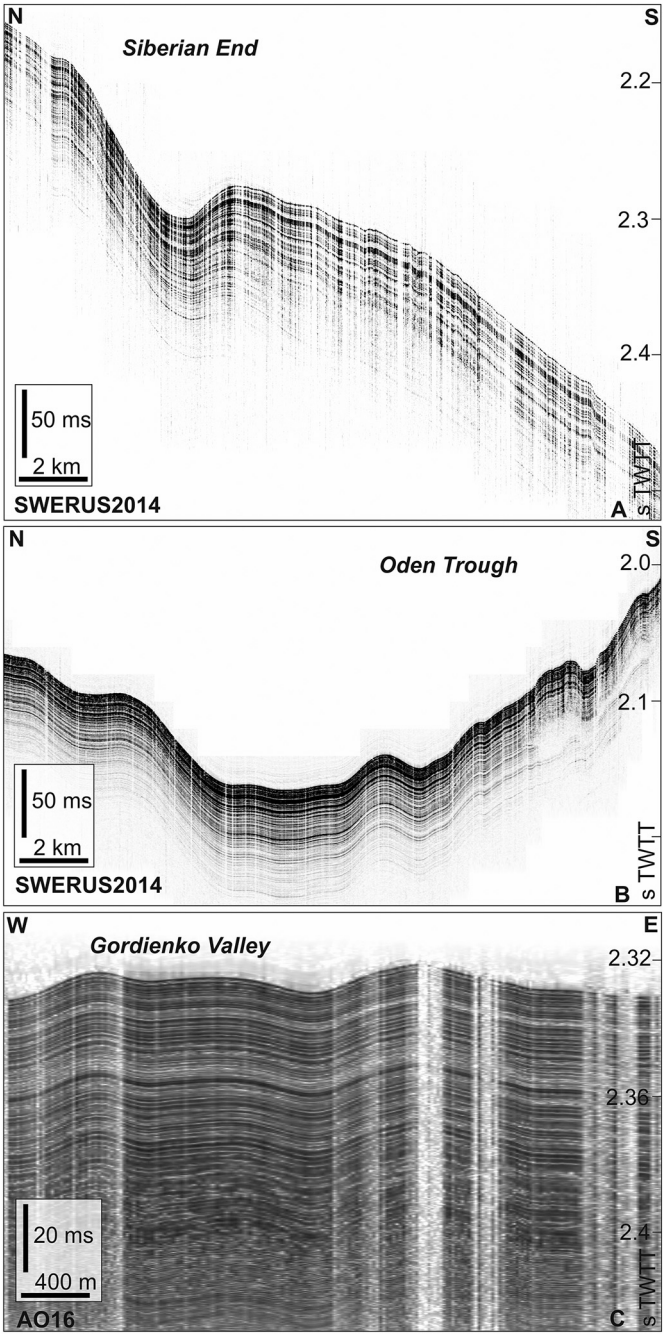

Fig. 10. Sub-bottom profile examples of sediment waves: A) Siberian End from the expedition SWERUS2014; B) Oden Trough from the expedition SWERUS2014; C) Gordienko Valley from the expedition AO16. For location see Fig. 2B. TWTT, two-way travel-time.

Basin adjacent to the Gakkel Ridge (Fig. 5B). It is referred to as the '*transparent layer*' and presents acoustic facies similar to the ones forming the MTDs (Fig. 9A). The transparent layer has a thickness of 5–7 m and thins towards the southwest (Fig. 9B). It is buried below 8–12 m of stratified sediments.

4.2. Sediment waves

The upper sedimentary record is locally undulated along the flank of Lomonosov Ridge facing Amundsen Basin (Fig. 5A). These undulations become more prominent in restricted areas forming a wavy pattern alike sediment waves (Fig. 5A, Fig. 10). The morphology of the sediment

Table 1
Average properties of the identified sediment waves.

Area	Depth range (m)	Length (km)	Height (m)
Siberian End	1000–1500	10	30
Oden Trough	1000–1500	2	20
	1500–2000	2-3	20
Belov Trough	1000–1500	>4	40
Gordienko Valley	1500–2000	>1	4
	2500–3000	>2	6
Amundsen Basin	>4000	12	6

The table colors allow to visualise the sediment waves at equivalent depth. The blue scale goes from light blue =shallow to dark blue=deep.

waves is variable, from relatively symmetric to asymmetric. The length of the waves varies from 1 to 10 km and their height from 4 to 40 m (Table 1). Generally, their crests appear to run parallel to the slope with the short flank holding the thicker layers and facing up-slope. The identified sediment waves are distributed over three depth ranges (Fig. 5A, Table 1): 1000–1500 m in the Belov Trough, Oden Trough and Siberian End; 1500–2000 m in the Gordienko Valley and Oden Trough; 2500–3000 m in the Gordienko Valley.

In addition, the stratified sedimentary record of the Amundsen Basin forms local sediment wave fields in the proximity to the Lomonosov Ridge at water depths over 4000 m (Fig. 5A, Table 1). The sediment waves in the Amundsen Basin are slightly asymmetric and about 12 km long and 6 m high. Their crests appear to be parallel to the slope with the short flank facing the ridge. Interleaved with the sediment waves, channel-like morphologies are identified at the base of Lomonosov Ridge (Fig. 5A). The channels are about 40 m deep relative to the surrounding seafloor and show levees that are more prominent on the abyssal plain side (Fig. 11).

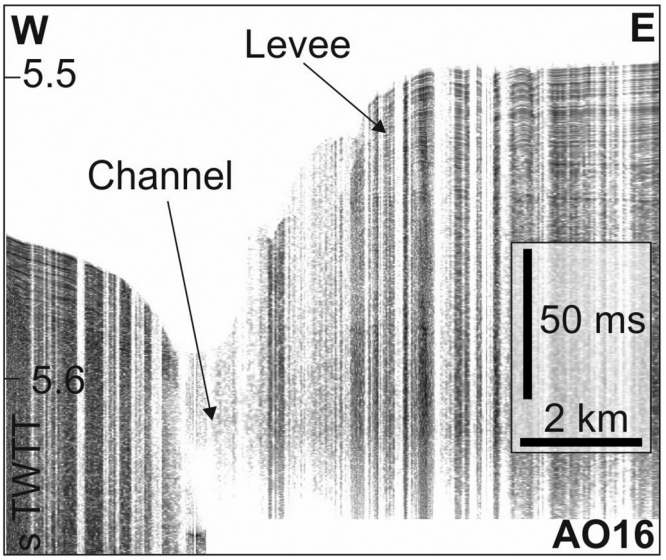

Fig. 11. Sub-bottom profile example from the expedition AO16 showing the interpreted channel at the base of Lomonosov Ridge. For location see Fig. 1B. TWTT, two-way travel-time.

5. Discussion

Stratified sediments form the uppermost sedimentary record of the Lomonosov Ridge and the Amundsen Basin. The late Quaternary sediment input is related to hemipelagic, biogenic, and/or ice-rafted processes (Sellén et al., 2008; O'Regan et al., 2019). A stratified sedimentary record is also identified in older deposits documented by multichannel seismic reflection data (e.g. Jokat, 2005; Castro et al., 2019). Within the late Quaternary stratified record, several sedimentary features are interleaved as a result of post-depositional processes that disturbed the original configuration (Fig. 5). These post-depositional processes are related to variations in the tectonic, oceanographic and cryospheric settings, determining the final product revealed in the present-day morphology and stratigraphy. Below we discuss potential processes involved in the formation of the distinguished sedimentary features and their implications.

5.1. Trigger processes of MTDs

Several studies focussing on the shallowest subsurface (Kristoffersen et al., 2007; Stein et al., 2017) and the stratigraphy of the central Arctic Ocean as presented in this study, show an abundance of MTDs formed during the late Quaternary along the Lomonosov Ridge and the adjoining Amundsen Basin (Fig. 5B). Here we discuss the main possible triggers of the instabilities generating MTDs in the central Arctic Ocean.

5.1.1. Cryospheric processes

The identified MTDs on the Lomonosov Ridge are particularly abundant in the Oden Trough and the Siberian End (Fig. 5B, Fig. 8). Multibeam bathymetry has shown that the seafloor in these areas has been scoured by glacial ice (Jakobsson et al., 2016). The three distinct acoustic units in the sedimentary record of these areas document a critical part of the glacial history of the Arctic Ocean (Fig. 3, Fig. 4). The blank-layer has been interpreted to consist of reworked sediments beneath relatively fast-moving grounded ice (Jakobsson et al., 2016). It is located above the truncation surface that is deeper at the Siberian End compared to at the ridge crest around Oden Trough (Fig. 3D, Fig. 4D). The truncation surface has been previously interpreted to be caused by grounding ice during MIS 6 (Jakobsson et al., 2016). It is likely that the base of the blank-layer, representing the truncation surface, marks the maximum depth of deformation in the sediments in response to the grounding and scouring of glacial ice. A pan-Arctic ice shelf has been proposed based on the intense ice scouring and related glacial morphology along the crest of the Lomonosov Ridge (Fig. 5A) (Jakobsson et al., 2016). The size and thickness of this ice shelf, as well as its pan-Arctic extent, are still under discussion (Jakobsson et al., 2016; Stein et al., 2017). However, the grounded ice on the Lomonosov Ridge and its later retreat may have triggered the formation of glaciogenic debris flows as suggested by Pickering and Hiscot (2016), which fall within the general definition of MTDs used here. Extended circum-Arctic ice sheets and shelves were present during MIS 6 or earlier glacial periods (Polyak et al., 2001; Jakobsson et al., 2010, 2014, 2016; Niessen et al., 2013; Stein et al., 2017) when the bathymetric highs of the Lomonosov Ridge acted as pinning points (Polyak et al., 2001; Jakobsson et al., 2010, 2016; Nilsson et al., 2017; Gasson et al., 2018). The inferred position of the ice-shelf edge derived from these publications suggests that the Oden Trough and the Siberian End were covered under a thick ice shelf during the penultimate glacial stage MIS 6. Thus, ice scouring during MIS 6 and the retreat of the ice shelf from both areas during the subsequent interglacial are suggested to have triggered the formation of the subsurface MTDs identified along the crest of the Lomonosov Ridge (Fig. 5B, Fig. 12).

While subsurface MTDs related to redeposition of sediments eroded by glacial ice (presumably during MIS 6) are widespread along the Lomonosov Ridge, outcropping MTDs are more common in the Oden Trough, i.e. at 84°–85°N (Fig. 5B, Fig. 8C) and suggest more recent triggers. During the last glacial cycles, including MIS 4 and the LGM, the central Arctic Ocean may have been covered by thick perennial sea ice or even a more limited ice shelf with rare breakups north of 84°N (Jakobsson et al., 2014; Xiao et al., 2015; North Atlantic/Arctic Ocean Sea Ice Model). However, biologic productivity around 80°N supports occasional formation of open areas (Xiao et al., 2015; Gasson et al., 2018). The extent of ice shelves during the last glacial cycle was more restricted than during the penultimate glaciation (MIS 6). The outcropping MTDs suggest some additional scouring of the Lomonosov Ridge during the last glacial cycles (MIS 4 and 2). The development of an ice shelf in the Amerasian Basin has been suggested based on a widespread hiatus in radiocarbon dated sediments during the LGM (Jakobsson et al., 2014), and by geophysical evidence for ice scouring on the Chukchi Plateau, Arlis Plateau and Mendeleev Ridge that is provisionally dated to MIS 4 (Jakobsson et al., 2014; Joe et al., 2020). The scouring of highs close to the Oden Through by shelf ice or large icebergs calved from it,

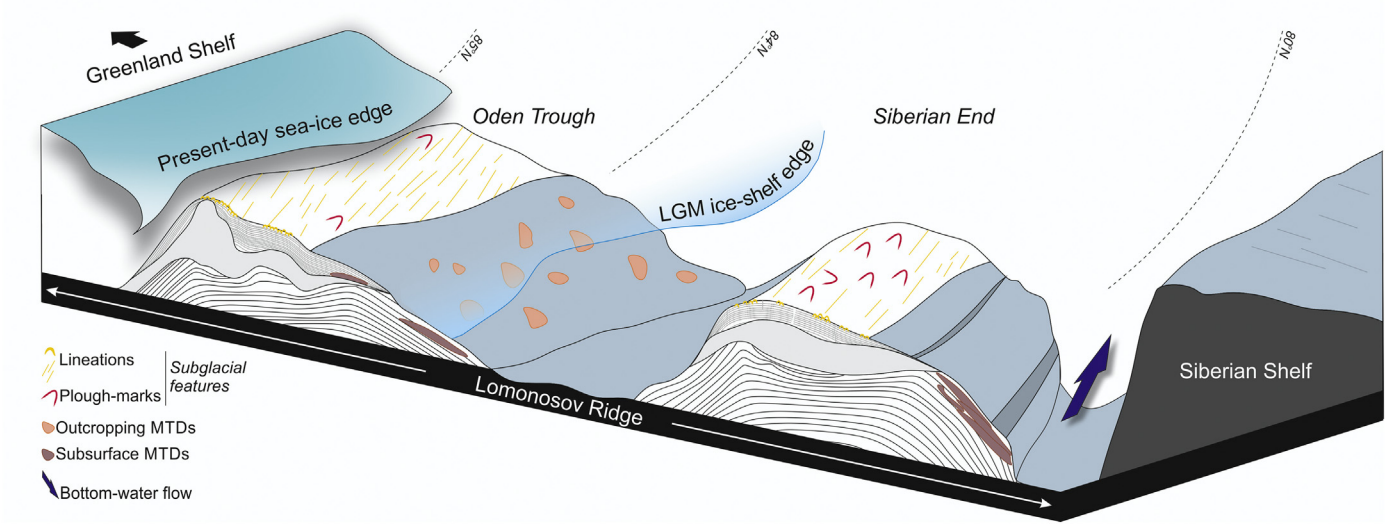

Fig. 12. Sketch of the identified sedimentary features at the Siberian End and in Oden Trough in relation to the ice sheet. Note that the estimated location of the ice sheet edge during Last Glacial Maximum (LGM) —— Marine Isotope Stage, MIS 2—— is marked, whereas a pan-Arctic ice sheet would occupy the area represented in the figure during MIS 6 according to Jakobsson et al. (2016) or at least the bathymetric highs (Stein et al., 2017).

may have triggered the formation of the outcropping MTDs in this area (Fig. 5B, Fig. 8C). Thus, the higher occurrence of outcropping MTDs in the Oden Trough, and their absence on the Siberian end, potentially indicates a more northerly position of the ice shelf edge in the central Arctic Ocean, or a different trajectory of large floating icebergs, compared to MIS 6 (Fig. 12). Both the blank-layer and the stratified-layer are thicker at the Siberian End than in Oden Trough (Fig. 3, Fig. 4) which may be either an artefact of increasing sedimentation rates as one approaches the Siberian shelf, or an indication that the seafloor close to the Siberian margin was less influenced by ice scouring during the last glacial cycle (Fig. 12).

5.1.2. Gas-hydrates destabilization

The distribution of MTDs over the central Arctic Ocean as described in the present work (Fig. 5B) may also reveal local destabilization of gas hydrates that were potentially embedded in the sedimentary record. Gas hydrates are stable in marine sediments at adequate pressure-temperature conditions and at the presence of a certain amount of organic carbon for microbial or thermogenic degradation (Xu and Ruppel, 1999; Tréhu et al., 2006). They are present globally on continental margins and slopes (e.g. Buffett and Archer, 2004; Klauda and Sandler, 2005), even though their amount and distribution remains poorly constrained (Beaudoin et al., 2014). The cold bottom water of the Arctic Ocean as well as its low geothermal gradient result in a relatively large volume of sediments with appropriate gas hydrate stability conditions (Stranne et al., 2016). The potential of large quantities of gas hydrates in the Arctic Ocean has been discussed in several studies (e.g. Kvenvolden and Grantz, 1990; Max and Lowrie, 1993; Max and Johnson, 2012).

An extensive Bottom Simulator Reflector (BSR) was previously identified in several multichannel seismic reflection profiles in a broad area of the central Arctic Ocean (Jokat, 2005), including the Oden Trough and the Siberian End (Fig. 1A). These two regions hold 83% of all MTDs identified in our study (Fig. 8). The identified BSR has a reversed polarity and is discordant with stratigraphic reflectors. Thus, it is tentatively considered as indirect evidence for the presence of gas hydrates (Jokat, 2005). The local destabilization of these hydrates could potentially result in the formation of the MTDs identified in our study (Fig. 5B, Fig. 6, Fig. 7). However, the nature of the BSR has been questioned after the development of a petrophysical model to calculate the pressure and temperature at the depth of the BSR (O'Regan and Moran, 2010). The model-inferred surface heat-flow is too high compared to regional data for the identified BSR to mark the base of the hydrate stability zone (O'Regan and Moran, 2010), i.e. the pressure-temperature phase boundary between the hydrate and free gas (e.g. Holbrook et al., 1996). Moreover, the constant depth of the identified BSR (2400 m) across a large geographic area (100,000 km^2; Jokat, 2005) argues against its relation to a geochemical front within hydrate bearing sediments (O'Regan and Moran, 2010).

Pore water chemistry studies along the Siberian margin also show a low potential for the presence of methane; with the exception of the Lomonosov Ridge (Miller et al., 2017). The estimated depth of the sulphate-methane transition, alkalinity and $\delta^{13}C$ of dissolved inorganic carbon of Lomonosov Ridge in the proximity of the Siberian End are close to the typical values of areas where methane is present in the sediments (Miller et al., 2017). Pockmarks related to gas migration have been identified previously on the Lomonosov Ridge and adjacent areas (Jakobsson et al., 2016; Jakobsson and O'Regan, 2016). In case of gas hydrate presence at the Oden Trough and the Siberian End, several freshwater events and inflow of warm Atlantic Water occurring since MIS 6 (Spielhagen, 2004), could have triggered the destabilization of the hydrates and the subsequent formation of MTDs. Therefore, although evidence for a hydrate-related BSR in this area is controversial, other evidence supports the possible presence of methane hydrates (Miller et al., 2017) and active fluid flow systems (i.e., pockmarks near Oden Trough (Jakobsson and O'Regan, 2016)), suggesting that a number of the MTDs identified at the Siberian End and in Oden Trough could be related to gas hydrate destabilization or fluid flow in the sediments.

5.1.3. Tectonics and other processes

Other sedimentary control factors, such as sea-level changes or high sediment accumulation are also important for the generation of MTDs (e.g. Maslin et al., 2004; Masson et al., 2010). Particularly along the flank of the Lomonosov Ridge such control factors are likely to have varied significantly, hence making the area prone for sediment instability (Fig. 5B, Fig. 8). High sediment accumulation and gravitational sliding could trigger the MTDs attached to the mound-like features at the flanks of Oden Trough (Fig. 7). Earthquakes and tectonic deformation are recognised worldwide as causes of MTD formation (e.g. Masson et al., 2006). However, the Lomonosov Ridge seems seismologically inactive since no earthquakes have been registered by the current circum-Arctic net of seismometers of the International Seismological Centre (ISC; Fig. 1A). Yet, due to the remote location of the ridge, earthquakes of magnitude below 4 are unlikely to be detected. The occurrence of MTDs on the Lomonosov Ridge could therefore be associated with recent tectonic activity that cannot be detected with the current distribution of seismometers around the Arctic Ocean. No evidence of such activity has been identified in the analysed data. Only a few fractures have been recognised in the Oden Trough (Supplementary Fig. 2). At the flank facing the Amundsen Basin, the fractures are located between 930 and 970 m water depth and at the flank facing Makarov Basin at water depths between 1015 and 1070 m. These fractures are therefore not geographically related to the MTDs (Fig. 1B, Fig. 5B).

The identified MTDs in Amundsen Basin are located in vicinity of the Gakkel Ridge that constitutes an active oceanic spreading centre, where a high number of earthquakes occur (Fig. 1A). Based on the mapped MTDs from the sparse data in the Amundsen Basin (Fig. 5B, Fig. 9A), the MTDs and the transparent layer identified in its recent sedimentary record are potentially related to the active seismicity along the Gakkel Ridge, i.e. the tectonic movement derived from the oceanic spreading of the ridge possibly triggers the formation of MTDs from unconsolidated sediments.

5.2. Sediment waves and oceanographic patterns

The sediment waves identified in the upper sedimentary record of the central Arctic Ocean respond to different potential processes of formation, i.e. turbidity currents, bottom currents and internal waves. Tidal processes have been previously suggested as a formation process (Polyak and Jakobsson, 2011). However, the low resolution of the available records has prevented a more detailed interpretation. The orientation of the identified sediment waves in the study area, parallel to the slope of the Lomonosov Ridge, suggests that they may have formed by turbidity currents flowing down-slope (Fig. 5A, Fig. 10). The dimensions of the identified sediment waves and in particular those within the Gordienko Valley are similar to those of sediment waves formed by turbidity currents in fine-grained sediments (Fig. 10, Table 1), i.e. a length under 7 km and a height up to 80 m (Wynn and Stow, 2002). The crests of the identified sediment waves are commonly aligned perpendicular to the flow direction and form on the right-hand levee relative to the current flow (Wynn and Stow, 2002). The channels identified at the base of the Lomonosov Ridge can be interpreted as turbidity channels originating at the Greenland margin (Fig. 11). They present a more prominent levee towards the abyssal plain similar to what is observed in the *North Pole Submarine Fan* (Fig. 1A) (Kristoffersen et al., 2004b). The dimensions of the sediment waves in the abyssal plain of the Amundsen Basin (Table 1) classify them as formed by soft sediment deformation (Wynn and Stow, 2002). They may relate to the flows passing through the turbidity channels towards the North Pole.

The morphology and internal structure of most of the identified sediment waves at the Lomonosov Ridge classify them as slightly migrating waves according to Hüneke and Mulder (2011), even though some of

them could be standing sediment waves. Turbidity current sediment waves involve active wave migration up-slope (Wynn and Stow, 2002; Faugères and Mulder, 2011). However, the dimensions of the sediment waves described along the slope of Lomonosov Ridge also fall within the classification of waves formed by bottom currents in fine-grained sediments (Wynn and Stow, 2002), i.e. a length under 10 km and a height up to 150 m. The sediment waves identified at the Siberian End and in Belov Trough fit particularly well with this type (Fig. 10, Table 1). Therefore, the formation of the identified sediment waves in the central Arctic Ocean should be most probably attributed to multi-process origin.

Up-slope migrating sediment waves have also been associated with the propagation of internal waves formed along the interfaces of the water masses (Faugères et al., 2002; Pomar et al., 2012; Ribó et al., 2016). Due to an orientation parallel to the slope, there are several examples of sediment waves associated with near-inertial internal waves, which were previously attributed to gravitational slope failure (e.g. Ribó et al., 2016).

The interface between the Atlantic Water and the Arctic Intermediate Water is placed at an approximate depth of 1000 m, while the interface between the Arctic Intermediate Water and the Arctic Ocean Deep Water varies between 1500 and 2000 m (Supplementary Fig. 1) (e.g. Gemery et al., 2017). The identified sediment waves at the flank of the Lomonosov Ridge facing the Amundsen Basin lie at the depth level of the water mass interfaces (Fig. 5A, Table 1). Thus, the identified sediment waves in this area could have been generated by interaction of the bathymetry with solitary internal waves that propagate and amplify along the interfaces between the Atlantic Water, the Arctic Intermediate Water and the Arctic Deep Water. In the Gordienko Valley, sediment waves at the flank of the Lomonosov Ridge occur at depths below 2000 m (Table 1), which may relate to a different circulation pattern of intermediate and deep waters in the Amundsen Basin. Below 2000 m, the deep water flows parallel to the Lomonosov Ridge reaching the vicinity of the Greenland Shelf (Fig. 1). In contrast, the flow of the intermediate water follows the Lomonosov Ridge up to the area of the North Pole, where it detaches and turns southeastwards towards the Fram Strait (Jones et al., 1995). The Gordienko Valley would be located to the south of the area of high interaction between the interfaces of intermediate waters and the morphology of the Lomonosov Ridge flank.

Based on the variety of processes that could explain the formation of the sediment waves in the central Arctic Ocean, and their occurrence at depths matching the water mass interfaces, we suggest internal waves as potential processes behind the formation of some of the sediment waves of the central Arctic Ocean. However, further research on the relation between sedimentary features and the flow of water masses in the Arctic Ocean is needed to constrain these interactions.

6. Conclusions

The morphology and stratigraphy of the central Arctic Ocean reveal sedimentary features that are related to post-depositional processes. The upper sedimentary record of the Lomonosov Ridge and Amundsen Basin has been influenced by the tectonic, oceanographic and cryospheric variability of the area during the late Quaternary. Seabed erosion associated with an oscillating ice sheet over the Arctic Ocean would generate mass transport deposits (MTDs) in the vicinity of areas subjected to ice grounding. The location of these sedimentary features along the Lomonosov Ridge denotes a progressive northward migration of the ice shelf edge during the last glacial cycles, from the Siberian margin towards the North Pole. The majority of these glaciogenic MTDs are buried in acoustically stratified sediments, and are consistent with glacial erosion during the penultimate glaciation. However, the recognition of outcropping MTDs in northern locations, may indicate more recent ice-scouring events during the last glacial cycle. The destabilization of gas hydrates cannot be ruled out as potential trigger of the MTDs. A tectonic triggering mechanism is suggested for the sparse MTDs identified in the abyssal plain of the Amundsen Basin, based on the proximity to the tectonically active Gakkel Ridge.

The presence of sediment waves along the flank of the Lomonosov Ridge facing the Amundsen Basin could be related to gravity driven downslope transport of sediments. Alternatively, the sediment waves may relate to internal waves occurring at the interfaces between the Atlantic Water and the Arctic Intermediate Water, and between the Arctic Intermediate Water and the Arctic Deep Water. The depth-match between these interfaces and the identified fields of sediment waves, together with the internal structure of the sediment waves, point to water mass interface-slope morphology interaction in the sediment wave formation. However, further research is needed to constrain this relation.

Supplementary data to this article can be found online at https://doi.org/10.1016/j.geomorph.2020.107309.

Declaration of competing interest

The authors declare that they have no known competing financial interests or personal relationships that could have appeared to influence the work reported in this paper.

Acknowledgements

This work has been developed under the framework of the *Geocenter Denmark* project: 'Sedimentary processes in the Arctic Ocean: tectonic, oceanographic and climatic implications' grant number 2-2017. Part of the data were made available by Canada and the Kingdom of Denmark who acquired the data for mapping their extended continental shelves under the legal framework of the United Nations Convention on the Law of the Sea (UNCLOS). Special mention to Stockholm University for providing access to the Swedish geophysical data. The first author acknowledges the 'Early Career Scientist programme on board Oden 2016' hosted by the Swedish Polar Research Secretariat, which allowed her participation in the expedition AO2016. We acknowledge the helpful comments and suggestions made by the two anonymous reviewers on the first version of this manuscript.

References

Aksenov, Y., Ivanov, V.V., Nurser, A.J.G., Bacon, S., Polyakov, I.V., Coward, A.C., Naveira-Garabato, A.C., Beszczynska-Moeller, A., 2011. The Arctic Circumpolar Boundary Current. J. Geophys. Res. 116 (C9).

Anderson, L.G., Björk, G., Holby, O., Jones, E.P., Kattner, G., Koltermann, K.P., Liljeblad, B., Lindegren, R., Rudels, B., Swift, J., 1994. Water masses and circulation in the Eurasian Basin: results from the Oden 91 expedition. 99 (C2), 3273–3283.

Backman, J., Moran, K., McInroy, D.B., Mayer, L.A., 2006. IODP, 302: Arctic Coring Expedition (ACEX). Proceedings of the Integrated Ocean Drilling Program 302. Integrated Ocean Drilling Program Management International, Inc., Edinburgh.

Beaudoin, Y.C., Waite, W., Boswell, R., Dallimore, S.R., 2014. Frozen heat: a UNEP global outlook on methane gas hydrates, 1. 1, 80.

Bijl, P.K., Houben, A.J.P., Hartman, J.D., Pross, J., Salabarnada, A., Escutia, C., Sangiorgi, F., 2018. Paleoceanography and ice sheet variability offshore Wilkes Land, Antarctica – part 2: insights from Oligocene–Miocene dinoflagellate cyst assemblages. Clim. Past 14 (7), 1015–1033.

Björk, G., Jakobsson, M., Rudels, B., Swift, J.H., Anderson, L., Darby, D.A., Backman, J., Coakley, B., Winsor, P., Polyak, L., Edwards, M., 2007. Bathymetry and deep-water exchange across the central Lomonosov Ridge at 88–89°N. Deep-Sea Res. I Oceanogr. Res. Pap. 54 (8), 1197–1208.

Björk, G., Jakobsson, M., Assmann, K., Andersson, L.G., Nilsson, J., Stranne, C., Mayer, L., 2018. Bathymetry and oceanic flow structure at two deep passages crossing the Lomonosov Ridge. Ocean Sci. 14 (1), 1–13.

Brozena, J.M., Childers, V.A., Lawver, L.A., Gahagan, L.M., Forsberg, R., Faleide, J.I., Eldholm, O., 2003. New aerogeophysical study of the Eurasia Basin and Lomonosov Ridge: implications for basin development. Geology 31 (9), 825–828.

Buffett, B., Archer, D., 2004. Global inventory of methane clathrate: sensitivity to changes in the deep ocean. Earth Planet. Sci. Lett. 227 (3–4), 185–199.

Cacchione, D.A., Pratson, L.F., Ogston, A.S., 2002. The shaping of continental slopes by internal tides. Science 296 (5568), 724–727.

Castro, C.F., Knutz, P.C., Hopper, J.R., Funck, T., 2019. Depositional evolution of the Western Amundsen Basin. Arctic Ocean: Paleoceanographic and Tectonic Implications 33 (12), 1357–1382.

Cochran, J.R., Edwards, M.H., Coakley, B.J., 2006. Morphology and structure of the Lomonosov Ridge, Arctic Ocean. Geochemistry, Geophysics, Geosystems 7 (5).

Colleoni, F., Krinner, G., Jakobsson, M., Peyaud, V., Ritz, C., 2009. Influence of regional parameters on the surface mass balance of the Eurasian ice sheet during the peak Saalian (140 kya). Glob. Planet. Chang. 68 (1), 132–148.

Darby, D.A., Polyak, L., Jakobsson, M., 2009. The 2005 HOTRAX Expedition to the Arctic Ocean. Glob. Planet. Chang. 68 (1–2), 1–4.

De Vernal, A., Eynaud, F., Henry, M., Hillaire-Marcel, C., Londeix, L., Mangin, S., Matthiessen, J., Marret, F., Radi, T., Rochon, A., Solignac, S., Turon, J.L., 2005. Reconstruction of sea-surface conditions at middle to high latitudes of the Northern Hemisphere during the Last Glacial Maximum (LGM) based on dinoflagellate cyst assemblages. Quat. Sci. Rev. 24 (7–9), 897–924.

Døssing, A., Jackson, H.R., Matzka, J., Einarsson, I., Rasmussen, T.M., Olesen, A.V., Brozena, J. M., 2013. On the origin of the Amerasia Basin and the High Arctic Large Igneous Province-results of new aeromagnetic data. Earth Planet. Sci. Lett. 363, 219–230.

Dowdeswell, J.A., Canals, M., Jakobsson, M., Todd, B.J., Dowdeswell, E.K., Hogan, K.A. (Eds.), 2016. Atlas of Submarine Glacial Landforms: Modern, Quaternary and Ancient. 46. Geological Society.

Engen, O., Eldholm, O., Bungum, H., 2003. The Arctic Plate Boundary. p. 108.

Faugères, J.-C., Mulder, T., 2011. Contour Currents and Contourite Drifts. 63.

Faugères, J.C., Zaragosi, S., Mezerais, M.L., Masse, L., 2002. The Vema contourite fan in the South Brazilian basin. Geological Society, London, Memoirs 22 (1), 209–222.

Gasson, E.G.W., DeConto, R.M., Pollard, D., Clark, C.D., 2018. Numerical simulations of a kilometre-thick Arctic ice shelf consistent with ice grounding observations. Nat. Commun. 9 (1), 1510.

Geissler, W.H., Jokat, W., Brekke, H., 2011. The Yermak Plateau in the Arctic Ocean in the light of reflection seismic data-implication for its tectonic and sedimentary evolution. Geophys. J. Int. 187 (3), 1334–1362.

Gemery, L., Cronin, T.M., Poirier, R.K., Pearce, C., Barrientos, N., O'Regan, M., Johansson, C., Koshurnikov, A., Jakobsson, M., 2017. Central Arctic Ocean paleoceanography from ~50 ka to present, on the basis of ostracode faunal assemblages from the SWERUS 2014 expedition. Clim. Past 13 (11), 1473–1489.

Gladenkov, A., Oleinik, A., Marincovich, L., Barinov, K.B., 2002. A Refined Age for the Earliest Opening of Bering Strait. 183.

Grosswald, M.G., Hughes, T.J., 2008. The case for an ice shelf in the pleistocene Arctic Ocean. Polar Geogr. 31 (1–2), 69–98.

Hebbeln, D., Dokken, T., Andersen, E.S., Hald, M., Elverhøi, A., 1994. Moisture supply for northern ice-sheet growth during the Last Glacial Maximum. Nature 370, 357.

Holbrook, W.S., Hoskins, H., Wood, W.T., Stephen, R.A., Lizarralde, D., 1996. Methane hydrate and free gas on the Blake Ridge from vertical seismic profiling. Science 273, 1840–1843.

Hughes, T., Denton, G.H., Grosswald, M.G., 1977. Was there a late-Würm Arctic Ice Sheet? Nature 266, 596.

Hüneke, H., Mulder, T., 2011. Deep-sea Sediments, Developments in Sedimentology. 63. Elsevier Science, Oxford.

Jakobsson, M., 1999. First high-resolution chirp sonar profiles from the central Arctic Ocean reveal erosion of Lomonosov Ridge sediments. Mar. Geol. 158 (1–4), 111–123.

Jakobsson, M., O'Regan, M., 2016. Pockmarks on the Mendeleev Rise, central Arctic Ocean. Geological Society, London, Memoirs 46 (1), 297–298.

Jakobsson, M., Backman, J., Rudels, B., Nycander, J., Frank, M., Mayer, L., Jokat, W., Sangiorgi, F., O'Regan, M., Brinkhuis, H., King, J., Moran, K., 2007. The early Miocene onset of a ventilated circulation regime in the Arctic Ocean. Nature 447 (7147), 986–990.

Jakobsson, M., Polyak, L., Edwards, M., Kleman, J., Coakley, B., 2008. Glacial geomorphology of the Central Arctic Ocean: the Chukchi Borderland and the Lomonosov Ridge. Earth Surf. Processes Landf. 33 (4), 526–545.

Jakobsson, M., Nilsson, J., O'Regan, M., Backman, J., Löwemark, L., Dowdeswell, J.A., Mayer, L., Polyak, L., Colleoni, F., Anderson, L.G., Björk, G., Darby, D., Eriksson, B., Hanslik, D., Hell, B., Marcussen, C., Sellén, E., Wallin, Å., 2010. An Arctic Ocean ice shelf during MIS 6 constrained by new geophysical and geological data. Quat. Sci. Rev. 29 (25–26), 3505–3517.

Jakobsson, M., Anderson, J.B., Nitsche, F.O., Dowdeswell, J.A., Gyllencreutz, R., Kirchner, N., Mohammad, R., O'Regan, M., Alley, R.B., Anandakrishnan, S., Eriksson, B., Kirshner, A., Fernandez, R., Stolldorf, T., Minzoni, R., Majewski, W., 2011. Geological record of ice shelf break-up and grounding line retreat, Pine Island Bay, West Antarctica. Geology 39 (7), 691–694.

Jakobsson, M., Mayer, L., Coakley, B., Dowdeswell, J.A., Forbes, S., Fridman, B., Hodnesdal, H., Noormets, R., Pedersen, R., Rebesco, M., Schenke, H.W., Zarayskaya, Y., Accettella, D., Armstrong, A., Anderson, R.M., Bienhoff, P., Camerlenghi, A., Church, I., Edwards, M., Gardner, J.V., Hall, J.K., Hell, B., Hestvik, O., Kristoffersen, Y., Marcussen, C., Mohammad, R., Mosher, D., Nghiem, S.V., Pedrosa, M.T., Travaglini, P.G., Weatherall, P., 2012. The International Bathymetric Chart of the Arctic Ocean (IBCAO) version 3.0. Geophysical Research Letters 39 (12), 6.

Jakobsson, M., Andreassen, K., Bjarnadóttir, L.R., Dove, D., Dowdeswell, J.A., England, J.H., Funder, S., Hogan, K., Ingólfsson, Ó., Jennings, A., Krog Larsen, N., Kirchner, N., Landvik, J.Y., Mayer, L., Mikkelsen, N., Möller, P., Niessen, F., Nilsson, J., O'Regan, M., Polyak, L., Nørgaard-Pedersen, N., Stein, R., 2014. Arctic Ocean glacial history. Quat. Sci. Rev. 92, 40–67.

Jakobsson, M., Nilsson, J., Anderson, L., Backman, J., Bjork, G., Cronin, T.M., Kirchner, N., Koshurnikov, A., Mayer, L., Noormets, R., O'Regan, M., Stranne, C., Ananiev, R., Barrientos Macho, N., Cherniykh, D., Coxall, H., Eriksson, B., Floden, T., Gemery, L., Gustafsson, O., Jerram, K., Johansson, C., Khortov, A., Mohammad, R., Semiletov, I., 2016. Evidence for an ice shelf covering the central Arctic Ocean during the penultimate glaciation. Nat. Commun. 7, 10365.

Joe, Y.J., Polyak, L., Schreck, M., Niessen, F., Yoon, S.H., Kong, G.S., Nam, S.I., 2020. Late Quaternary depositional and glacial history of the Arliss Plateau off the East Siberian margin in the western Arctic Ocean. Quat. Sci. Rev. 228, 106099.

Jokat, W., 2005. The sedimentary structure of the Lomonosov Ridge between 88°N and 80°N. Geophys. J. Int. 163 (2), 698–726.

Jokat, W., Uenzelmann-Neben, G., Kristoffersen, Y., Rasmussen, T.M., 1992. Lomonosov Ridge—a double-sided continental margin. Geology 20 (10), 887–890.

Jones, E.P., Rudels, B., Anderson, L.G., 1995. Deep waters of the Arctic Ocean: origins and circulation. Deep-Sea Res. I 42 (5), 737–760.

Klauda, J., Sandler, S., 2005. Global Distribution of Methane Hydrate in Ocean Sediment. p. 19.

Knies, J., Cabedo-Sanz, P., Belt, S.T., Baranwal, S., Fietz, S., Rosell-Mele, A., 2014. The emergence of modern sea ice cover in the Arctic Ocean. Nat. Commun. 5, 5608.

Kristoffersen, Y., Coakley, B., Jokat, W., Edwards, M., Brekke, H., Gjengedal, J., 2004a. Seabed erosion on the Lomonosov Ridge, central Arctic Ocean: a tale of deep draft icebergs in the Eurasia Basin and the influence of Atlantic water inflow on iceberg motion? Paleoceanography 19 (3) (n/a-n/a).

Kristoffersen, Y., Sorokin, M.Y., Jokat, W., Svendsen, O., 2004b. A submarine fan in the Amundsen Basin, Arctic Ocean. Mar. Geol. 204 (3–4), 317–324.

Kristoffersen, Y., J. Coakley, B., Hall, J., Edwards, M., 2007. Mass Wasting on the Submarine Lomonosov Ridge, Central Arctic Ocean, 243.

Kvenvolden, K.A., Grantz, A., 1990. Gas hydrates of the Arctic Ocean region. In: Grantz, A., Johnson, L., Sweeney, J.F. (Eds.), The Arctic Ocean Region. Geological Society of America.

Lovell, B., 2010. A pulse in the planet: regional control of high-frequency changes in relative sea level by mantle convection. J. Geol. Soc. 167 (4), 637–648.

Marcussen, C., the LOMROG II Scientific Party, 2009. Lomonosov Ridge off Greenland 2009 (LOMROG III) – Cruise Report. Geological Survey of Denmark and Greenland report 2011/106 (154 pp.).

Marcussen, C., the LOMROG III Scientific Party, 2012. Lomonosov Ridge off Greenland 2012 (LOMROG III) – Cruise Report. Geological Survey of Denmark and Greenland Report 2012/119 (222 pp.).

Marincovich, L., Gladenkov, A., 1999. Evidence for an Early Opening of the Bering Strait. 397 pp. 149–151.

Marincovich, L., Gladenkov, A., 2001. New evidence for the age of Bering Strait. Quat. Sci. Rev. 20, 329–335.

Maslin, M., Owen, M., Day, S., Long, D., 2004. Linking continental-slope failures and climate change: testing the clathrate gun hypothesis. Geology 32 (1), 53–56.

Masson, D.G., Harbitz, C.B., Wynn, R.B., Pedersen, G., Lovholt, F., 2006. Submarine landslides: processes, triggers and hazard prediction. Philosophical transactions. Series A, Mathematical, Physical, and Engineering Sciences 364 (1845), 2009–2039.

Masson, D.G., Wynn, R.B., Talling, P.J., 2010. Large landslides on passive continental margins: processes, hypotheses and outstanding questions. In: Mosher, D., Shipp, R.C., Moscardelli, L., Chaytor, J., Baxter, C.P., Lee, H., Urgeles, R. (Eds.), Submarine Mass Movements and Their Consequences. Advances in Natural and Technological Hazards Research. Springer Netherlands, pp. 153–165.

Max, M.D., Johnson, A.H., 2012. Natural Gas Hydrate (NGH) Arctic Ocean Potential Prospects and Resource Base. 2.

Max, M.D., Lowrie, A., 1993. Natural gas hydrates: Arctic and Nordic Sea potential. In: e.a. T. O. Vorren (Ed.), Arctic Geology and Petroleum Potential, NPF Special Publication 2. Elsevier, Amsterdam, pp. 27–53.

Mercer, J.H., 1970. A Former Ice Sheet in the Arctic Ocean? 8

Mienert, J., Weaver, P.P.E., 2002. European Margin Sediment Dynamics. Springer, Berlin.

Miller, C.M., Dickens, G.R., Jakobsson, M., Johansson, C., Koshurnikov, A., Regan, M., Muschitiello, F., Stranne, C., Mörth, C.-M., 2017. Pore water geochemistry along continental slopes north of the East Siberian Sea: inference of low methane concentrations. Biogeosciences 14 (12), 2929–2953.

Moran, K., Backman, J., Brinkhuis, H., Clemens, S.C., Cronin, T., Dickens, G.R., Eynaud, F., Gattacceca, J., Jakobsson, M., Jordan, R.W., Kaminski, M., King, J., Koc, N., Krylov, A., Martinez, N., Matthiessen, J., McInroy, D., Moore, T.C., Onodera, J., O'Regan, M., Pälike, H., Rea, B., Rio, D., Sakamoto, T., Smith, D.C., Stein, R., St John, K., Suto, I., Suzuki, N., Takahashi, K., Watanabe, M., Yamamoto, M., Farrell, J., Frank, M., Kubik, P., Jokat, W., Kristoffersen, Y., 2006. The Cenozoic palaeoenvironment of the Arctic Ocean. Nature 441 (7093), 601–605.

Mosher, D.C., Shipp, R.C., Moscardelli, L., Chaytor, J.D., Baxter, C.D.P., Lee, H.J., Urgeles, R. (Eds.), 2010. Submarine Mass Movements and Their Consequences. Advances in Natural and Technological Hazards Research. 28. Springer.

Mosher, D.C., Shimeld, J., Hutchinson, D., Lebedeva-Ivanova, N., Chapman, C.B., 2012. Submarine Landslides in Arctic Sedimentation: Canada Basin. Submarine Mass Movements and Their Consequences. Springer Netherlands, Dordrecht, pp. 147–157.

Mulder, T., Cochonat, P., 1996. Classification of offshore mass movements. J. Sediment. Res. 66 (1), 43–57.

Nelson, C.H., Escutia, C., Damuth, J.E., Twichell, D.C., 2011. Interplay of mass-transport and turbidite-system deposits in different active tectonic and passive continental margin settings: external and local controlling factors. In: Shipp, R.C., Weimer, P., Posamentier, H.W. (Eds.), Mass-transport Deposits in Deepwater Settings. SEPM (Society for Sedimentary Geology), Broken Arrow USA, pp. 39–66.

Niessen, F., Hong, J.K., Hegewald, A., Matthiessen, J., Stein, R., Kim, H., Kim, S., Jensen, L., Jokat, W., Nam, S.-I., Kang, S.-H., 2013. Repeated Pleistocene glaciation of the East Siberian continental margin. Nat. Geosci. 6, 842.

Nikishin, A.M., Gaina, C., Petrov, E.I., Malyshev, N.A., Freiman, S.I., 2017. Eurasia Basin and Gakkel Ridge, Arctic Ocean: crustal asymmetry, ultra-slow spreading and continental rifting revealed by new seismic data. Tectonophysics 746, 64–82.

Nilsson, J., Jakobsson, M., Borstad, C., Kirchner, N., Björk, G., Pierrehumbert, R.T., Stranne, C., 2017. Ice-shelf damming in the glacial Arctic Ocean: dynamical regimes of a basin-covering kilometre-thick ice shelf. Cryosphere 11 (4), 1745–1765.

O'Regan, M., King, J., Backman, J., Jakobsson, M., Pälike, H., Moran, K., Heil, C., Sakamoto, T., Cronin, T.M., Jordan, R.W., 2008. Constraints on the Pleistocene chronology of sediments from the Lomonosov Ridge. 1st ed. 23 Paleoceanography and Paleoclimatolog.
O'Regan, M., Moran, K., 2010. Deep water methane hydrates in the Arctic Ocean: reassessing the significance of a shallow BSR on the Lomonosov Ridge. J. Geophys. Res. 115 (B5).
O'Regan, M., Backman, J., Barrientos, N., Cronin, T.M., Gemery, L., Kirchner, N., Mayer, L.A., Nilsson, J., Noormets, R., Pearce, C., Semiletov, I., Stranne, C., Jakobsson, M., 2017. The De Long Trough: a newly discovered glacial trough on the East Siberian continental margin. Clim. Past 13 (9), 1269–1284.
O'Regan, M., Coxall, H.K., Cronin, T.M., Gyllencreutz, R., Jakobsson, M., Kaboth, S., Löwemark, L., Wiers, S., West, G., 2019. Stratigraphic Occurrences of Sub-Polar Planktic Foraminifera in Pleistocene Sediments on the Lomonosov Ridge, Arctic Ocean. Frontiers in Earth Science. 7.
Payton, C.E., 1977. Seismic stratigraphy-applications to hydrocarbon exploration. American Association of Petroleum geologists, Tulsa, Okla. 26, 516.
Pease, V., Drachev, S., Stephenson, R., Zhang, X., 2014. Arctic lithosphere — a review. Tectonophysics 628, 1–25.
Pickering, K.T., Hiscot, R.N. (Eds.), 2016. Deep Marine Systems. Processes, Deposits, Environments, Tectonics and Sedimentation. AGU & Wiley.
Polyak, L., Jakobsson, M., 2011. Quaternary sedimentation in the Arctic Ocean: recent advances and further challenges. Oceanography 24 (3), 52–64.
Polyak, L., Edwards, M.H., Coakley, B.J., Jakobsson, M., 2001. Ice shelves in the Pleistocene Arctic Ocean inferred from glaciogenic deep-sea bedforms. Nature 410 (6827), 453–457.
Polyak, L., Alley, R.B., Andrews, J.T., Brigham-Grette, J., Cronin, T.M., Darby, D.A., Dyke, A.S., Fitzpatrick, J.J., Funder, S., Holland, M., Jennings, A.E., Miller, G.H., O'Regan, M., Savelle, J., Serreze, M., St. John, K., White, J.W.C., Wolff, E., 2010. History of sea ice in the Arctic. Quat. Sci. Rev. 29 (15–16), 1757–1778.
Pomar, L., Morsilli, M., Hallock, P., Bádenas, B., 2012. Internal waves, an under-explored source of turbulence events in the sedimentary record. Earth Sci. Rev. 111 (1–2), 56–81.
Potter, P.E., Szatmari, P., 2009. Global Miocene tectonics and the modern world. Earth Sci. Rev. 96 (4), 279–295.
Raymo, M.E., 1994. The initiation of Northern Hemisphere glaciation. Annual Review of Earth & Planetary Sciences 22, 353–383.
Reading, H.G. (Ed.), 1996. Sedimentary Environments. Processes, Facies and Stratigraphy. Blackwell Science.
Rebesco, M., Hernández-Molina, F.J., Van Rooij, D., Wåhlin, A., 2014. Contourites and associated sediments controlled by deep-water circulation processes: state of the art and future considerations. Mar. Geol. 352, 111–154.
Ribó, M., Puig, P., Muñoz, A., Lo Iacono, C., Masqué, P., Palanques, A., Acosta, J., Guillén, J., Gómez Ballesteros, M., 2016. Morphobathymetric analysis of the large fine-grained sediment waves over the Gulf of Valencia continental slope (NW Mediterranean). Geomorphology 253, 22–37.
Rudels, B., 2009. Arctic Ocean Circulation, Encyclopedia of Ocean Sciences. Elsevier Ltd, pp. 211–225.
Rudels, B., Muench, R.D., Gunn, J., Schauer, U., Friedrich, H.J., 2000. Evolution of the Arctic Ocean boundary current north of the Siberian shelves. J. Mar. Syst. 25 (1), 77–99.
Sangiorgi, F., Brumsack, H.-J., Willard, D.A., Schouten, S., Stickley, C.E., O'Regan, M., Reichart, G.-J., Sinninghe Damsté, J.S., Brinkhuis, H., 2008. A 26 million year gap in the central Arctic record at the greenhouse-icehouse transition: looking for clues. Paleoceanography 23 (1), PA1S04.
Sarnthein, M., Bartoli, G., Prange, M., Schmittner, A., Schneider, B., Weinelt, M., Andersen, N., Garbe-Schönberg, D., 2009. Mid-Pliocene shifts in ocean overturning circulation and the onset of Quaternary-style climates. Clim. Past Discuss. 5 (2), 269–283.
Sekretov, S.B., 2002. Structure and tectonic evolution of the Southern Eurasia Basin, Arctic Ocean. Tectonophysics 351 (3), 193–243.
Sellén, E., Jakobsson, M., Backman, J., 2008. Sedimentary regimes in Arctic's Amerasian and Eurasian Basins: Clues to differences in sedimentation rates. Glob. Planet. Chang. 61 (3–4), 275–284.
Sher, A., 1995. Is there any real evidence for a huge shelf ice sheet in East Siberia? Quat. Int. 28, 39–40.
Shipp, R.C., Weimer, P., Posamentier, H.W. (Eds.), 2011. Mass-transport Deposits in Deepwater Settings. SEPM Special Publication 96. SEPM (Society for Sedimentary Geology).
Sohn, R.A., Willis, C., Humphris, S., Shank, T.M., Singh, H., Edmonds, H.N., Kunz, C., Hedman, U., Helmke, E., Jakuba, M., Liljebladh, B., Linder, J., Murphy, C., Nakamura, K.I., Sato, T., Schlindwein, V., Stranne, C., Tausenfreund, M., Upchurch, L., Winsor, P., Jakobsson, M., Soule, A., 2008. Explosive volcanism on the ultraslow-spreading Gakkel ridge, Arctic Ocean. Nature 453 (7199), 1236–1238.
Somavilla, R., Schauer, U., Budéus, G., 2013. Increasing amount of Arctic Ocean deep waters in the Greenland Sea. Geophys. Res. Lett. 40 (16), 4361–4366.
Spielhagen, R., 2004. Arctic Ocean deep-sea record of northern Eurasian ice sheet history. Quat. Sci. Rev. 23 (11—13), 1455–1483.
Stein, R., Fahl, K., Müller, J., 2012. Proxy reconstruction of Cenozoic Arctic Ocean sea-ice history - from IRD to IP25. Polarforschung 82 (1), 37–71.
Stein, R., Fahl, K., Schreck, M., Knorr, G., Niessen, F., Forwick, M., Gebhardt, C., Jensen, L., Kaminski, M., Kopf, A., Matthiessen, J., Jokat, W., Lohmann, G., 2016. Evidence for ice-free summers in the late Miocene central Arctic Ocean. Nat. Commun. 7, 11148.
Stein, R., Fahl, K., Gierz, P., Niessen, F., Lohmann, G., 2017. Arctic Ocean sea ice cover during the penultimate glacial and the last interglacial. Nat. Commun. 8 (1), 373.
Stevenson, R., Poirier, A., Véron, A., Carignan, J., Hillaire-Marcel, C., 2015. Late Eocene to present isotopic (Sr–Nd–Pb) and geochemical evolution of sediments from the Lomonosov Ridge, Arctic Ocean: implications for continental sources and linkage with the North Atlantic Ocean. Compt. Rendus Geosci. 347 (5–6), 227–235.
Stranne, C., O'Regan, M., Dickens, G.R., Crill, P., Miller, C., Preto, P., Jakobsson, M., 2016. Dynamic simulations of potential methane release from East Siberian continental slope sediments. Geochem. Geophys. Geosyst. 17 (3), 872–886.
Svindland, K.T., Vorren, T.O., 2002. Late Cenozoic sedimentary environments in the Amundsen Basin, Arctic Ocean. Mar. Geol. 186 (3–4), 541–555.
Tréhu, A.M., Bangs, N.L., Guerin, G., 2006. Near-offset vertical seismic experiments during Leg 204. In: Tréhu, A.M., Bohrmann, G., Torres, M.E., Colwell, F.S. (Eds.), Proc. ODP, Sci. Results, College Station, TX (Ocean Drilling Program), pp. 1–23.
Vogt, P.R., Crane, K., Sundvor, E., 1994. Deep Pleistocene iceberg plowmarks on the Yermak Plateau: Sidescan and 3.5 kHz evidence for thick calving ice fronts and a possible marine ice sheet in the Arctic Ocean. Geology 22 (5), 403–406.
Woodgate, R.A., Aagaard, K., Muench, R.D., Gunn, J., Björk, G., Rudels, B., Roach, A.T., Schauer, U., 2001. The Arctic Ocean Boundary Current along the Eurasian slope and the adjacent Lomonosov Ridge: water mass properties, transports and transformations from moored instruments. Deep-Sea Res. I Oceanogr. Res. Pap. 48 (8), 1757–1792.
Wynn, R.B., Masson, D.G., 2008. Sediment Waves and Bedforms.
Wynn, R.B., Stow, D.A.V., 2002. Classification and characterisation of deep-water sediment waves. Mar. Geol. 192 (1–3), 7–22.
Wynn, R.B., Masson, D.G., Stow, D.A.V., Weaver, P.P.E., 2000. Turbidity current sediment waves on the submarine slopes of the western Canary Islands a SOES, Southampton Oceanography Centre, Uníersity of Southampton, Empress Dock. Mar. Geol. 163, 185–198.
Xiao, X., Stein, R., Fahl, K., 2015. MIS 3 to MIS 1 temporal and LGM spatial variability in Arctic Ocean sea ice cover: reconstruction from biomarkers. Paleoceanography 30 (7), 969–983.
Xu, W., Ruppel, C., 1999. Predicting the Occurrence, Distribution, and Evolution of Methane Gas Hydrate in Porous Marine Sediments. 104.